

# RECENT RESULTS FROM PEP\*

R. Hollebeek

Stanford Linear Accelerator Center  
Stanford University,  
Stanford, California 94305, U.S.A.

## ABSTRACT

Preliminary results are presented for the data taken by the MARK II and MAC collaborations at the PEP storage ring. Results include measurements of QED processes, limits on the weak couplings  $g_V$  and  $g_A$ , limits on anomalous lepton production, the measurement of the  $\tau$  lifetime, scale violation in inclusive hadron production, Monte Carlo independent tests of QCD using energy-energy correlations and single jet energy moments, measurements of the properties of three jet events, and measurements of proton, neutral kaon, lambda and proton pair yields.

## INTRODUCTION

The PEP storage ring began serious operation for physics in January of 1981. In the six months of operation between January and June, it has produced  $16,000 \text{ nb}^{-1}$  of integrated luminosity at 29 GeV in the center-of-mass. Average luminosity per shift varied between 40 and  $70 \text{ nb}^{-1}$  during this time with a record of  $370 \text{ nb}^{-1}$  collected in one three-shift period.

During this time, the interaction regions were occupied by the experiments shown in Table 1. Data presented in this talk were accumulated by the MARK II and MAC collaboration and are preliminary. The MARK II detector (see fig. 1) was debugged by operating for one year at the SPEAR storage ring and was moved to PEP when the ring was completed. This has eliminated the need for a long check-out period with this detector at the new storage ring and has allowed the group to rapidly analyze the data which have only been available for a few months. The MAC detector (fig. 2) covers a large solid angle with electromagnetic and hadronic calorimetry. The acceptance extends to  $|\cos\theta| = 0.95$  which is large compared to many previous experiments. This large acceptance increases the efficiency for event detection and also decreases the model dependence of efficiency corrections.

The Free Quark Search and Monopole Search results are

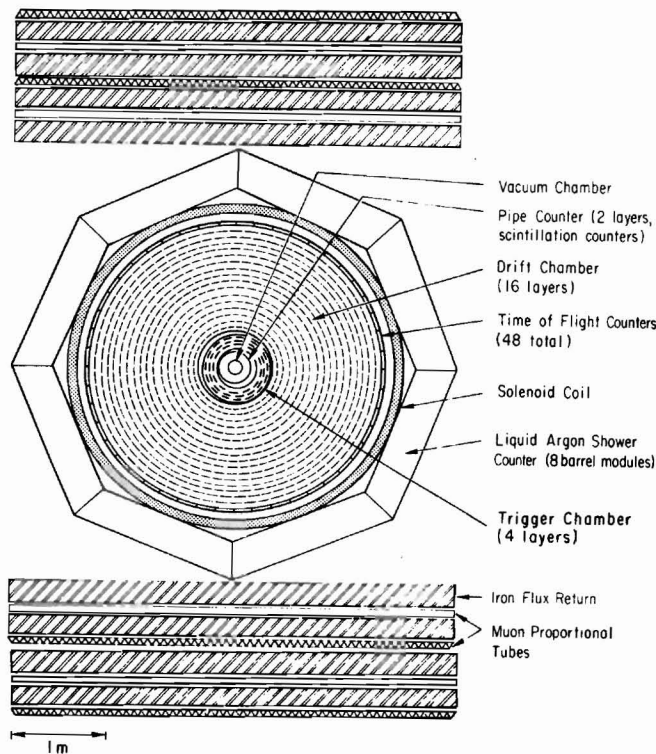


Fig. 1. MARK II Detector.

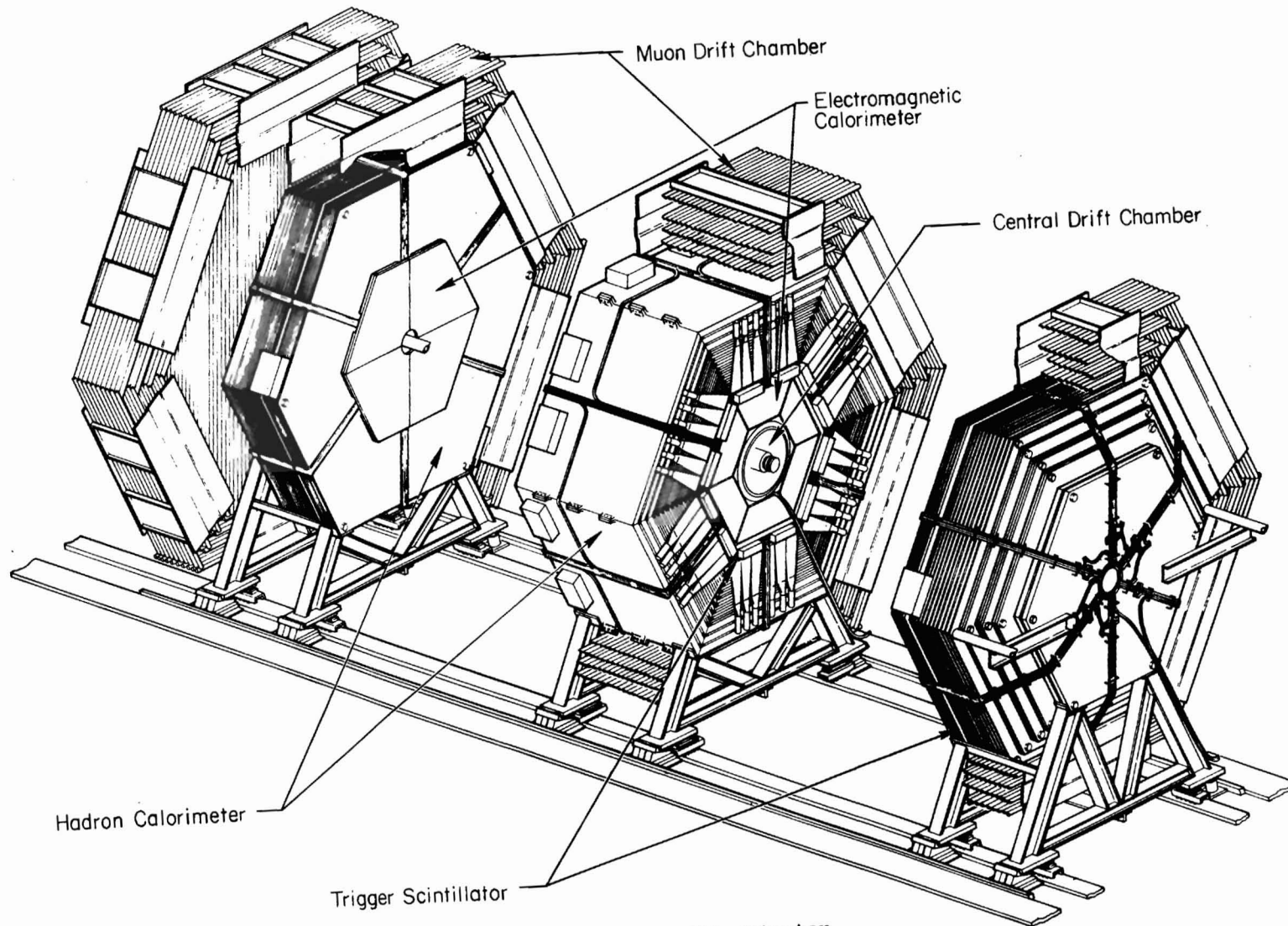


Fig. 2. MAC Detector.

TABLE 1

<u>Interaction Region</u>	<u>Experiment</u>	<u>Purpose</u>
2	PEP-9	Forward Detector Facility for 2 gamma physics
4	PEP-6	MAC--Calorimetric Detector
6	PEP-14	Free Quark Search
8	PEP-20	DELCO--Cerenkov Detector
10	PEP-2	Monopole Search using LEXAN and CR-39 plastic
12	PEP-5	MARK II - General Purpose Detector

reported by A. Litke at this conference. The PEP-9 experiment (fig. 3) is designed to observe two-photon reactions using a pair of small angle detectors. It is designed to be used with the Time Projection Chamber experiment (PEP-4) which is not yet installed. Proportional wire chambers and the PEP-4 inner drift chamber were installed in the central region for the January-June cycle to assist in check-out of the detector. Machine studies of the septum magnets with compensating skew quadrupoles were done and the machine can now run with these magnets energized. The DELCO experiment (fig. 4) is also being checked out and has accumulated approximately  $9000 \text{ nb}^{-1}$  for this purpose. The Cerenkov cells in this detector will allow it to separate low energy electrons and K mesons and assist in the analysis of charmed and bottom mesons produced at high energy. The DELCO collaboration has also installed a set of quadrupoles known as mini-beta 1 which are capable of decreasing the  $\beta$  function to approximately 10 cm in interaction region 8 and hence increasing the luminosity there. Machine studies of these magnets were begun in June.

During the 1981 summer shutdown at PEP, the closest quadrupoles to the interaction regions (Q1) were moved in all IR's from their design positions

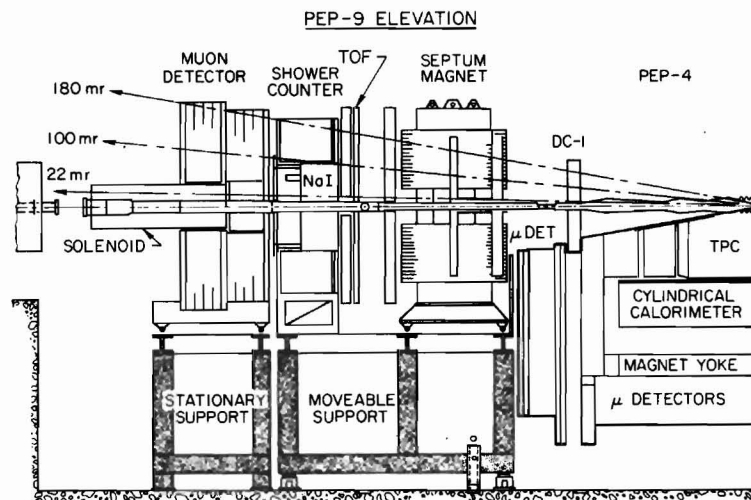


Fig. 3. PEP-9 Forward Detector.

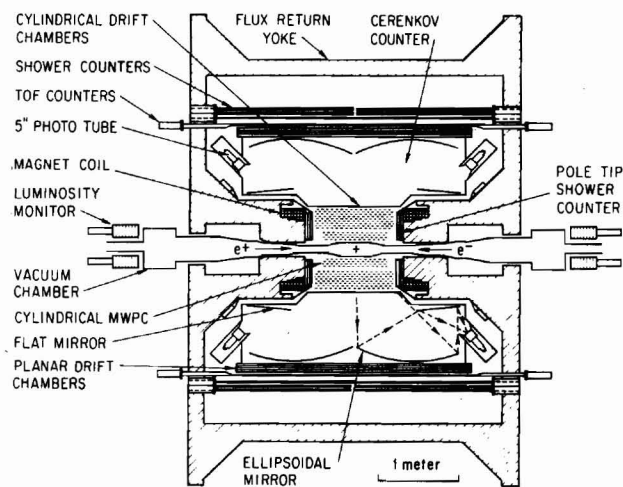


Fig. 4. DELCO Detector

at 11 meters to new positions 7.4 meters from the interaction point. Calculations indicate that the move will reduce the  $\beta_y^*$  at the interaction region by at least a factor of 2 and thus increase the luminosity by the same factor. The Free Quark Search experiment was removed from interaction region 6 and the High Resolution Spectrometer experiment using the 2 meter diameter magnet of the Argonne 12 foot Bubble Chamber was installed in its place.

A great deal of physics has already been produced by the MAC and MARK II collaborations using the data obtained in the first six months of PEP operation and with the increased luminosity available from the movement of the IR quadrupoles and the additional capabilities of the experiments newly installed or completing their check-out we can look forward to much more in the coming months.

QED TESTS AND SEARCHES FOR ANOMALOUS LEPTON PRODUCTION

The high energies available at electron-positron storage rings provide a clean testing ground for Quantum Electrodynamics (QED). This theory has been phenomenally successful at predicting the features of low energy atomic structure, fine and hyperfine splittings, the properties of muonium, and the magnetic moments of electrons and muons. Many of these processes are measured very precisely and calculated to high order in the coupling constant  $\alpha$ . While the low energy measurements test our ability to calculate to high order within the framework of the theory, high energy reactions, since they involve very large momentum transfers, provide tests of the assumed point-like nature of the interacting particles. No test so far has given an indication that the theory is incorrect and it remains the most severely tested and most successful theory in physics today.

Three types of tests have been performed at PEP. The first test uses the cross-sections and angular distributions of the reactions

$$\begin{aligned}
 e^+e^- &\rightarrow e^+e^- \\
 e^+e^- &\rightarrow \mu^+\mu^- \\
 e^+e^- &\rightarrow \tau^+\tau^- \\
 e^+e^- &\rightarrow \gamma\gamma
 \end{aligned}$$

to test the point-like nature of the leptons  $e$ ,  $\mu$  and  $\tau$ , and give limits on modifications of the photon propagator and in the case of  $e^+e^- \rightarrow \gamma\gamma$ , limits on modifications to the electron propagator. The second type of test is a search for evidence of the contributions of the weak interactions. Unified theories of the weak and electromagnetic interactions predict modifications to most QED reactions because of the coupling of the weak neutral current to leptons. The third test is a search for new sources of lepton production. Here again it will be shown that the known leptons and QED provide a satisfactory explanation for the leptons seen in  $\mu e$  events and  $\mu\gamma$  events where heavy leptons or excited leptons might contribute.

ee +  $\gamma\gamma$

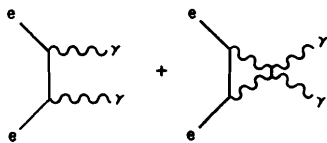


Fig. 5. QED diagrams for  $e^+e^- \rightarrow \gamma\gamma$

The lowest order diagram for this cross section involves the t channel exchange of an electron as shown in fig. 5. This channel is unique among the two body QED final states in that it is not modified to lowest order by the weak interactions.<sup>1</sup> Modifications to lowest order QED behavior can be parametrized by the form

$$\frac{d\sigma}{d\Omega} = \frac{d\sigma_0}{d\Omega} \left( 1 \pm \frac{s^2 \sin^2 \theta}{2\Lambda_{\pm}^4} \right)$$

where

$$\frac{d\sigma_0}{d\Omega} = \frac{\alpha^2}{s} \left( \frac{1 + \cos^2 \theta}{\sin^2 \theta} \right)$$

The  $\Lambda_{\pm}$  parameter can be interpreted as a limit on the contribution of a heavy electron with mass  $m_{E^*}$  and charge  $e^*$  in which case we have  $\Lambda_{\pm} = m_{E^*} \sqrt{e/e^*}$ .

Events for this test are collected with total energy triggers based on the electromagnetic calorimeters of the MAC and MARK II detectors. The event topology requires the back-to-back deposit of energy in two calorimeters. The MAC detector requires the total energy deposit to be in the range  $14.5 < E < 40$  GeV and has a total luminosity of  $7040 \text{ nb}^{-1}$ . The MARK II detector requires  $19 < E < 35$  GeV and has a sample of  $15,400 \text{ nb}^{-1}$ . Radiative corrections are applied to the lowest order cross-section using  $\gamma\gamma$  and  $\gamma\gamma\gamma$  events generated by the Kleiss-Berends Monte Carlo.<sup>2</sup> Both analyses require that no tracks are seen in the chambers in front of the deposited energy and hence must be corrected for the conversion of photons in the material of the beam pipe. For the MARK II the material in front of the main drift chambers represents  $\sim 10\%$  of a radiation length. The resulting bin by bin correction to the observed cross section is

$$\frac{1}{1 - \frac{0.0056}{\sin^2 \theta}}$$

The cross-section together with the QED expected cross section to order  $\alpha^3$  for the MARK II and MAC detectors are shown in figs. 6 and 7, respectively.

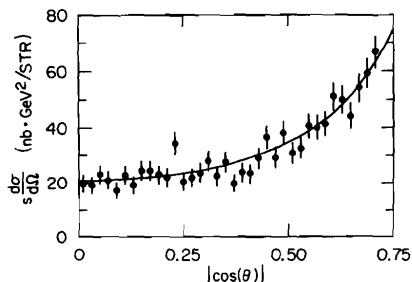


Fig. 6. MARK II  $e^+e^- \rightarrow \gamma\gamma$  data with QED to order  $\alpha^3$ .

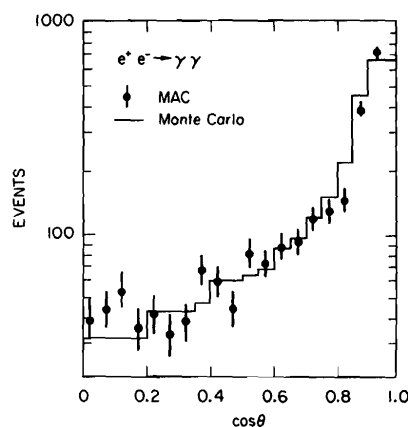


Fig. 7 MAC  $e^+e^- \rightarrow \gamma\gamma$  data with QED to order  $\alpha^3$ .

For the MARK II detector, the values of  $\Lambda_{\pm}$  are determined by a  $\chi^2$  minimization procedure. For each value of  $\Lambda$ , the  $\chi^2$  is minimized with respect to one parameter which is the overall normalization. The 95% confidence level is the value of  $\Lambda$  for which the  $\chi^2$  is four units larger than the value obtained for  $\Lambda \rightarrow \infty$ . The values obtained are shown in

Table II together with similar results from PETRA experiments.<sup>3</sup> The PLUTO and MARK J groups have also fit for a modification of the  $ee \rightarrow \gamma\gamma$  cross section of the form

TABLE 2 QED  $\Lambda$  Parameters for  $e^+e^- \rightarrow \gamma\gamma$

	$\Lambda_{\pm}$	neutral	
		$\Lambda_+$	$\Lambda_-$
MARK II	50	41	
CELLO	47	44	
MARK J	51	49	51 41
PLUTO	46		46 36
TASSO	34	42	

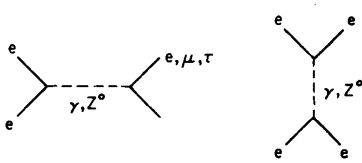
$$\frac{d\sigma}{d\Omega} = \frac{d\sigma_0}{d\Omega} \left( 1 \pm \frac{s^2 \sin^4 \theta}{2\Lambda_{\pm}^4 (1 + \cos^2 \theta)} \right)$$

corresponding to the inclusion of a neutral object which couples to fermions. Here again the limits are of order 40-50 GeV, and are shown in Table 2.

#### $ee \rightarrow ee$ and $ee \rightarrow \mu\mu$

The cross section for the production of lepton pairs is expected to be modified by the neutral weak current. In addition to the normal QED diagrams, diagrams must be included where the photon has been replaced by the neutral weak boson  $Z^0$  as shown in fig. 8.

The weak contributions to the  $\mu$  pair and  $e$  pair cross sections have been calculated by R. Budny<sup>4</sup> including the effects of initial state polarization and final state helicities. For the  $\mu$  pair cross section the result is of the form



$$\frac{d\sigma}{d\cos\theta} = \frac{\pi\alpha^2}{2s} [ F_1(1+\cos^2\theta) + F_2 \cos\theta ]$$

where

$$F_1 = 1 - 8 g_V^2 g_S \left( \frac{M_Z^2}{M_Z^2 - s} \right) + 16 (g_A^2 + g_V^2)^2 g_S^2 s^2 \left( \frac{M_Z^2}{M_Z^2 - s} \right)^2$$

$$F_2 = - 16 g_A^2 g_S \left( \frac{M_Z^2}{M_Z^2 - s} \right) + 128 g_A^2 g_V^2 g_S^2 s^2 \left( \frac{M_Z^2}{M_Z^2 - s} \right)$$

$$g = 4.49 \cdot 10^{-5} \text{ GeV}^{-2} .$$

Fig. 8. Weak and Electromagnetic Diagrams for lepton pair production.

An analysis of weak interaction experiments<sup>5</sup> gives

$$g_V^e = 0.043 \pm 0.063$$

$$g_A^e = -0.545 \pm 0.056 .$$

With these values, we can see that the weak effects make a very small change in the total  $\mu$  pair cross section ( $\sim .1\%$ ) while contributing a measurable effect via  $F_2$  to the front-back asymmetry

$$A = \frac{\frac{d\sigma}{d\Omega}(\theta) - \frac{d\sigma}{d\Omega}(\pi-\theta)}{\frac{d\sigma}{d\Omega}(\theta) + \frac{d\sigma}{d\Omega}(\pi-\theta)} .$$

This asymmetry is negative below the  $z$  pole.

For the electron-pair final state, the value of  $g_V$  changes the total cross section and the form of the angular distribution at the several percent level. Therefore care must be taken that there are no systematic problems in the absolute normalization. The greatest sensitivity to  $g_V$  comes from the ratio of the normalizations of the Bhabha and muon pair cross sections since increasing  $g_V^2$  increases the Bhabha cross section but decreases the muon cross section (due to the negative coefficient in the second term of  $F_1$ ).

To be sensitive to effects on the cross-sections at the few percent level, it is important to include higher order effects in QED itself. Radiative effects

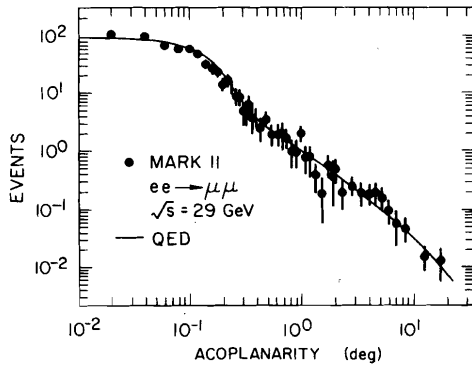


Fig. 9. MARK II Acoplanarity Distribution for  $\mu$  pairs compared to Berends-Kleiss QED predictions.

also modify the total cross section and in the case of the  $\mu$  pairs, the interference of the one photon ( $C = -1$ ) and two photon ( $C = +1$ ) intermediate states also generates an asymmetry which depends to some extent on the cuts used in the analysis. Both the MAC and the MARK II groups use the Berends-Kleiss Monte Carlo to produce samples of radiative events which can then be analyzed to find corrections for detector acceptances and efficiencies. An interesting test of the radiative correction calculations is the acoplanarity distribution of muon pairs since the distribution could not be calculated for example in the peaking approximation. This distribution is shown in fig. 9 for the  $\mu$  pairs from the MARK II. The theoretical curve is the order  $\alpha^3$  QED distribution normalized to the wide angle electron pairs.

The electron pair data from the MAC detector are shown in fig. 10. The data are corrected for radiative effects, and the

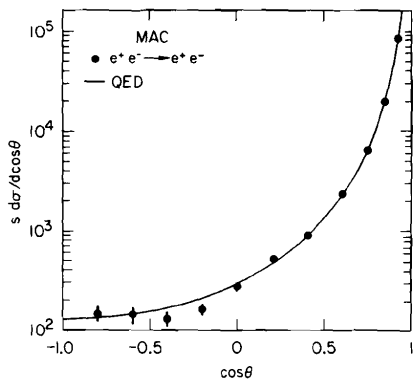


Fig. 10. MAC  $e^+e^- \rightarrow e^+e^-$ . Data are corrected for radiative effects. The curve is lowest order QED.

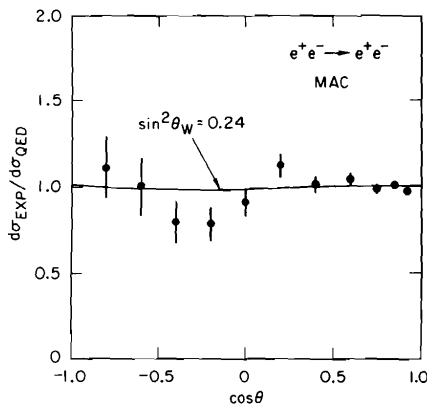


Fig. 11. MAC  $e^+e^- \rightarrow e^+e^-$  with QED subtracted.

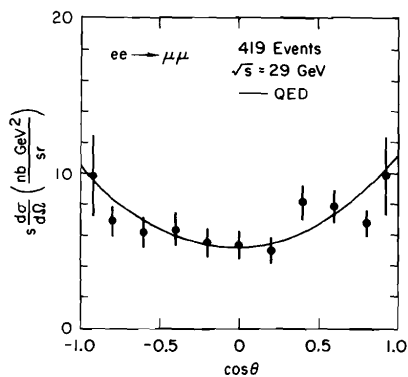


Fig. 12. MAC  $e^+e^- \rightarrow \mu^+\mu^-$  angular distribution.

curve shown is the lowest order cross section. The integrated luminosity is  $4400 \text{ nb}^{-1}$  with an acceptance determined by  $|\cos\theta| < 0.95$  which yields 19,600 events. The trigger requires two electromagnetic showers ( $E > 1.5 \text{ GeV}$ ) in back-to-back shower modules. The total shower energy is required to be greater than 14.5 GeV and there must be two oppositely charged tracks in the event which are collinear to within  $10^\circ$ . The data are fit using a  $\chi^2$  minimization to a Weinberg-Salam model with a single parameter  $\sin^2\theta_W$ . Figure 11 shows the ratio of the measured cross section to the QED cross section together with the results of the fit which gives  $\sin^2\theta_W = 0.24 \pm 0.16$  with a  $\chi^2$  of 22.3 for 10 degrees of freedom.

For the muon pair cross section, the MAC collaboration uses a collinearity cut of  $10^\circ$ . To eliminate muon pairs from the reaction  $ee \rightarrow ee\mu\mu$ , the sum of the magnitudes of the muon momenta must be greater than 8 GeV. The electromagnetic shower modules are used to remove Bhabha events and the final sample contains 419 events from a luminosity of  $7900 \text{ nb}^{-1}$ . The muon pair angular distribution is shown in fig. 12.

From the expression for the muon pair cross section given earlier, one finds that the asymmetry expected from weak effects is

$$8 g_A^2 g_s \frac{M_Z^2}{s - M_Z^2} \frac{x}{1 + x^2/3}$$

where  $x = |\cos\theta_{\text{max}}|$ . From this one can see that you expect to have an asymmetry which is about 50% larger in a detector of the MAC type which covers most of the  $\cos\theta$  range as compared to the more typical device which extends out to  $\cos\theta \sim .7$ . This increased  $\cos\theta$  range also increases the size of the radiative QED correction which must be applied to the data. For the MAC detector, the QED expected asymmetry is +2.7%. After subtraction, the asymmetry in the muon pairs from the MAC detector is

$$A = -0.009 \pm 0.052 \pm 0.015,$$

or

$$g_A^2 = 0.04 \pm 0.22$$

To obtain the maximum amount of information about possible weak effects, it is necessary to do a simultaneous fit to the electron and muon pair cross sections. This has been done by the MARK II collaboration on a sample of data which contains 878  $\mu$  pairs and 12,337 Bhabhas. The integrated luminosity used is  $14,480 \text{ nb}^{-1}$ .

Events are allowed to have up to four charged particles in order to minimize corrections to the normalization due to showering Bhabhas in the material of the detector. Within the event there must be a pair of oppositely charged particles, each with momentum  $p > 5.5 \text{ GeV/c}$  which are collinear to within  $20^\circ$ . The acceptance is defined by  $|\cos\theta| < 0.70$ .

Figure 13 shows the scatter plot of energy deposited in the liquid argon shower modules for the two tracks and indicates that  $\mu$  and  $e$  pairs

can be easily and cleanly separated in the detector. The separation is accomplished by requiring that a muon be a track which deposits only minimum ionizing energy in the liquid argon ( $E < 1.5$  GeV). With the above cuts, the contamination of  $\tau$  pairs in the  $\mu$  pair sample is estimated to be 3% and the contamination due to Bhabhas is a negligible 0.3%. The angular distribution for the Bhabha and muon cross-sections together with the expected cross section to order  $\alpha^3$  in QED are shown in figs. 14 and 15.

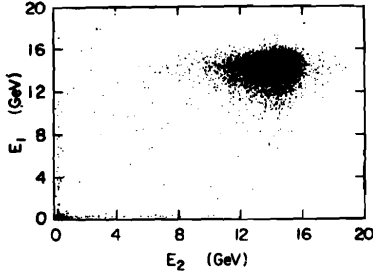


Fig. 13. MARK II scatter plot of energy deposition in two track events.

Using the cross sections and the luminosity as measured by the small angle monitors, a maximum likelihood fit is done for the values of  $g_V$ ,  $g_A$ , and a correction to the luminosity normalization. The result is

$$\begin{aligned} \mathcal{L} &= 14332 \pm 170 \text{ nb}^{-1} \\ g_A^2 &= 0.24 \pm 0.16 \\ |g_V| &= 0.22^{+0.17}_{-0.22} \end{aligned}$$

The QED subtracted cross sections are shown in Figs. 16 and 17 with the results of the fit. Figure 16 also shows the expected cross section dependence for the Weinberg-Salam model with  $\sin \theta_W = 0.23$  and for the case where the roles of  $g_V$  and  $g_A$  have been reversed, i.e.  $g_A \approx 0$ ,  $g_V^2 \approx .25$ . The muon cross section has also been fit independently. The normalization is allowed to float, and a maximum likelihood fit is made holding  $g_A$  fixed and assuming

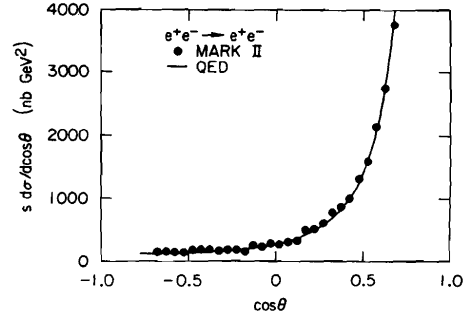


Fig. 14. MARK II  $e^+e^- \rightarrow e^+e^-$  data with  $\alpha^3$  QED prediction.

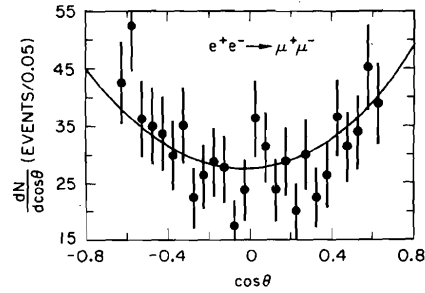


Fig. 15. MARK II  $e^+e^- \rightarrow \mu^+\mu^-$  angular distribution with  $\alpha^3$  QED prediction.

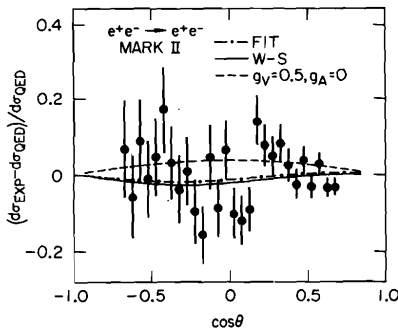


Fig. 16. QED subtracted cross section for  $e^+e^- \rightarrow e^+e^-$ , MARK II.

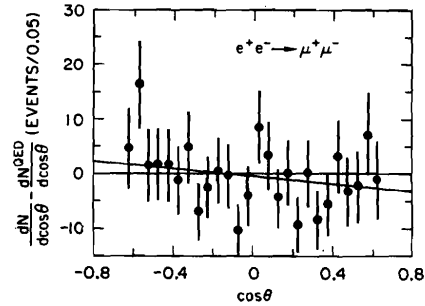


Fig. 17. QED subtracted cross section for  $e^+e^- \rightarrow \mu^+\mu^-$ , MARK II.

$M_z = \infty$ . The result is

$$g_A^2 = 0.38 \pm 0.18 \pm 0.02 .$$

### ee + $\tau\tau$

The MAC collaboration has used the  $\mu e$  sample to measure the cross section for the production of  $\tau$  pairs. The  $\mu$  and  $e$  must be collinear to within  $90^\circ$  and must have a momentum  $0.5 < p < 14.5$  GeV/c. The  $\cos\theta$  acceptance extends to 0.95. The result for the  $\tau$  angular distribution is shown in fig. 18. Background from  $ee + ee\tau\tau$  within this sample has been calculated to be six events. The result for the branching ratio product is

$$B(\tau \rightarrow e\nu\nu) B(\tau \rightarrow \mu\nu\nu) = 0.032 \pm 0.005 \pm 0.006 .$$

Assuming  $\mu$ - $e$  universality this yields a leptonic branching ratio for the  $\tau$

$$B(\tau \rightarrow \mu\nu\nu) = 0.176 \pm 0.015 \pm 0.018 .$$

The large solid angle of the MAC detector is important in this result because it results in a large increase in the detection efficiency for the acollinear  $\mu e$  topology. Although statistics are limited at the moment, this cross section will provide interesting tests in the future of  $\tau$ - $\mu$ - $e$  universality, limits on the point-like nature of  $\tau$ 's from the total cross section, and measurements of the weak axial coupling of the  $\tau$  from its angular asymmetry.

### Limits for anomalous lepton production

Both the MAC and MARK II collaborations have used the  $\mu e$  events to place limits on the presence of heavy leptons in the data. The advantage of using  $\mu e$  events is that the only model dependent calculation required is the calculation of the leptonic branching fraction. The approach of the two groups is similar. Kinematic cuts must be used to eliminate the contribution of events from the two photon production of  $ee\mu\mu$  events. The MARK II requires the momentum of each track to be greater than 1.5 GeV/c to eliminate this background. The MAC collaboration calculates the  $\beta$  of the missing momentum vector along the beam direction

$$\beta_z = \frac{P_z^\mu + P_z^e}{\sqrt{s} - E_\mu - E_e} .$$

The  $ee\mu\mu$  events tend to have large missing momentum along the beam ( $z$ ) direction and hence are eliminated by the cut  $|\beta_z| < .5$ . Sensitivity to high mass lepton pair production comes from the fact that high mass objects would generate a large relative transverse momentum between the  $e$  and the  $\mu$ . The measures of  $p_\perp$  used by the two collaborations are shown in fig. 19a,b.

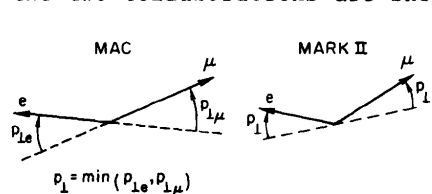


Fig. 19. Definition of  $p_\perp$  used by MAC and MARK II for the Heavy Lepton Search.

The  $p_\perp$  distributions are shown in figs. 20 and 21. Both groups find the total number of events and the momentum distributions to be consistent with that expected from the production of  $\tau$  pairs. The 95% C.L. limits from MAC is that the heavy lepton must have a mass greater than 14 GeV/c. The limit from the MARK II collaboration is  $M_{H.L.} > 13.8$  GeV/c.

The same data used to set  $H.L.$  limits on heavy leptons can be used to set limits on spin zero mesons which decay into  $e\nu$  and  $\mu\nu$ .

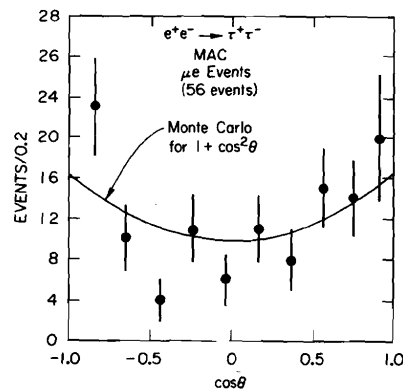


Fig. 18. MAC angular distribution for  $e^+e^- \rightarrow \tau^+\tau^-$  from  $\mu e$  events.

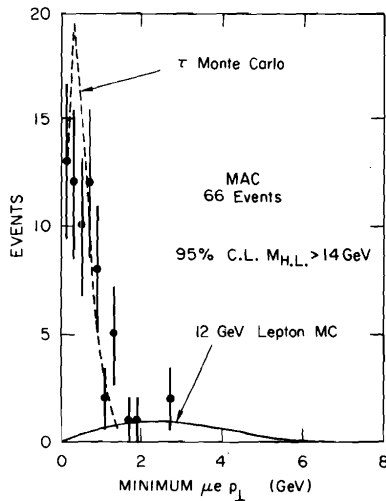


Fig. 20. MAC  $\mu e p_{\perp}$  distribution with expected curve from a 12 GeV Heavy Lepton.

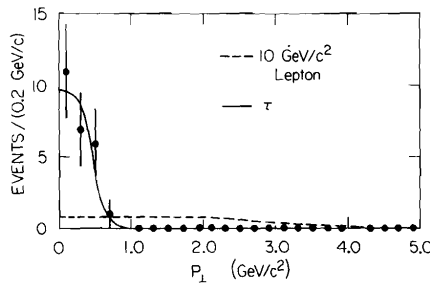


Fig. 21. MARK II  $\mu e p_{\perp}$  distribution.

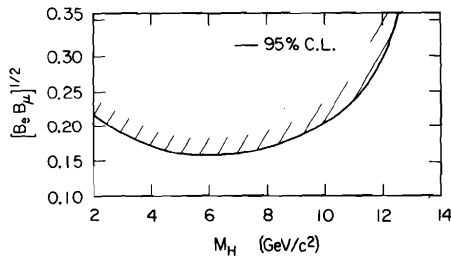


Fig. 22. MARK II Limit for Spin Zero Boson decaying to  $\mu\nu\nu$ .

and  $B_{\mu\gamma} = (\text{branching ratio of } \mu^* \rightarrow \mu\gamma)$  derived from the absence of  $\mu\mu\gamma\gamma$  is shown in fig. 23 as a function of the mass of the  $\mu^*$ . The 20 events with a single photon are explained by conventional sources with  $18.2 \pm 1.9$  events from radiative  $\mu$  pairs and  $0.3 \pm 0.1$  events from radiative  $\tau$  pairs.

A similar search has been performed by the MAC collaboration. Events with two identified muons and a single photon are selected from a sample representing a luminosity of  $8560 \text{ nb}^{-1}$ . The photon energy must be between 3 GeV and 14 GeV, and the angle between the beam axis and the photon must be greater than  $20^\circ$ . To further limit the contribution from radiative events, the angle between the

Charged Higgs particles or techni-pions<sup>6</sup> are examples of spin zero bosons which are produced with one quarter unit of R and a  $\beta^3$  threshold behavior. The most likely decay in these particular models is to  $\tau\nu$  and unfortunately no limit can be set even for 100% branching ratio to  $e$  and  $\mu$ . The limit from the MARK II for a spin zero boson decaying with branching ratio  $B_e, B_\mu$  to  $e\nu$  and  $\mu\nu$  respectively is shown in fig. 22 as a function of the boson mass  $M_H$ .

Limits on  $\mu^* \rightarrow \mu\gamma$

QED processes can also increase the observed yield of leptons if there exist excited states within the available energy range which can decay via photon emission. Excited electron states are already eliminated by the limits placed on the electron propagator in the process  $ee \rightarrow \gamma\gamma$ . For an equivalent test in the muon system, however, it is necessary to investigate the  $\mu\mu\gamma$  and  $\mu\mu\gamma\gamma$  yields directly.

The MARK II collaboration has used a sample of events with two oppositely charged particles both of which are identified as muons. Both muons must have a momentum  $p > 2.0 \text{ GeV}/c$  and the acoplanarity angle between the muons must satisfy

$$2^\circ < \theta_{\text{ACOPL}} < 175^\circ.$$

In order to reject the planar  $\mu\mu\gamma$  events coming from radiation corrections to the  $\mu$  pair cross sections, the quantity

$$P = \frac{(\vec{p}^+ \times \vec{p}^-) \cdot \vec{p}^0}{|\vec{p}^+ \times \vec{p}^-| |\vec{p}^0|}$$

must satisfy  $P > 0.02$ . (For a planar event one would find  $P = 0$ .) Photons used in the search are required to have energy  $E_\gamma > 2.0 \text{ GeV}$  and must be separated from any charged particle by at least  $0.33 M$  at the entrance to the liquid argon modules where they are detected.

With a luminosity of  $14,781 \text{ nb}^{-1}$ , these cuts yield 20  $\mu\mu\gamma$  events. The 95% confidence limit on the product

$$B_{\mu\gamma}^2 R_{\mu^*}$$

where

$$R_{\mu^*} = \frac{\sigma_{\mu^*\mu^*}}{\sigma_{\mu\mu}}$$

photon and either of the muons must be greater than  $20^\circ$ . One muon must be in the central region of the detector  $60^\circ < \theta < 120^\circ$  and the other must be in the range  $18.2^\circ < \theta < 161.8^\circ$ . The expected number of events from QED sources is 26 events and the observed number of events is also 26. The  $\mu\gamma$  invariant mass distribution (for a sample defined by slightly looser cuts and containing 40 events) is shown in fig. 24 and agrees well with the distribution calculated from QED.

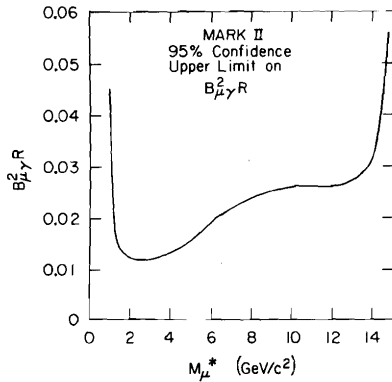


Fig. 23. MARK II limit for  $\mu^*$  production.

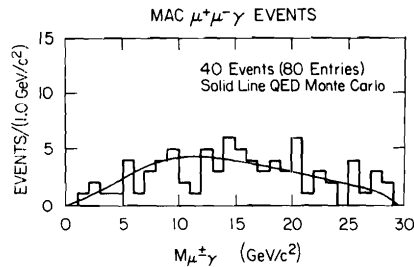


Fig. 24. MAC  $\mu\gamma$  invariant mass distribution for  $\mu^*$  search with QED prediction.

#### $\tau$ LIFETIME

The MARK II detector has measured the lifetime of the  $\tau$  lepton. Using a sample of 1500 produced  $\tau^+\tau^-$  pairs at 29 GeV, the decays of the  $\tau$  with three charged particles are used to construct a decay vertex. The distribution of decay vertices yields the flight path of a 14.5 GeV  $\tau$  lepton and hence its lifetime.

The lifetime of the  $\tau$  lepton is interesting because it provides a direct test of the coupling of the  $\tau$  to the charged weak current. If the  $\tau$  had the same coupling to this current as the  $\mu$ , then the lifetime of the  $\tau$  could be calculated from that of the muon. This  $\tau$ - $\mu$  universality calculation yields

$$\tau_\tau = \left( \frac{m_\mu}{m_\tau} \right)^5 \tau_\mu B_e = (2.8 \pm 0.2) 10^{-13} \text{ sec}$$

where the error comes from the uncertainty in the branching ratio  $B_e$  for  $\tau$  decaying to  $e\nu\nu$ . The measured value from the MARK II detector is

$$\tau_\tau = (4.6 \pm 1.9) 10^{-13} \text{ sec}$$

which indicates that at the one standard deviation level, the  $\tau$  coupling to the weak charged current is 0.66 to 1.02 times the value expected from  $\tau$ - $\mu$  universality.

In order to make this measurement, we have relied on two small hemicylindrical drift chambers which were installed close to the beam pipe. The addition of these chambers improves the ability to locate the  $\tau$  decay vertex by 30 to 50% over what it would have been using the main drift chamber only. The small chambers were added to the MARK II detector in order to improve the detector rejection of beam gas backgrounds and cosmic rays at the trigger level and hence they are referred to as the trigger chamber.

Each hemicylinder contains four layers of 32 axial sense wires. The chamber is 86 cm long and the inner and outer sense wire radii are 16.6 and 20.2 cm respectively. The main drift chamber has 16 layers, six of which are axial. The remaining layers of the main chamber are at  $\pm 3^\circ$  relative to the beam direction for use as small angle stereo layers. Both chambers have resolutions of

order 0.2 mm at each layer, but for this measurement the trigger chamber data have been analyzed as if they had a resolution of 0.3 mm to allow for possible small misalignments between the chambers. The rms momentum resolution of the trigger chamber-drift chamber combination on 14.5 GeV/c muons is  $0.6\% p^2$  if the track is constrained to pass through the beam position and  $0.8\% p^2$  if, as in this measurement, the constraint is not made.

The  $\tau$  leptons used for this study are produced by the reaction

$$e^+ e^- \rightarrow \tau^+ \tau^- .$$

Candidate events are required to have either four or six charged particles. Each event was divided into two jets by the plane normal to the sphericity axis, and at least one jet must have exactly three charge particles with net charge  $\pm 1$ . To reduce backgrounds from beam-gas interactions and two-photon  $\tau$  production, the visible energy of the event must be greater than  $0.125 E_{\text{c.m.}}$ . In addition, each event must have either an identified electron or muon or must have a visible energy greater than  $0.25 E_{\text{c.m.}}$ . Backgrounds from hadron production are reduced by requiring the invariant mass from the particles in each jet to be small; less than  $1.6 \text{ GeV}/c^2$  calculated from the charged particles and less than  $1.8 \text{ GeV}/c^2$  calculated from charged plus photons. Finally, to eliminate backgrounds from radiative Bhabha events, the invariant mass of a three prong jet must be greater than  $0.3 \text{ GeV}/c^2$  when all three particles are assumed to be electrons. The total energy measured by the tracking system or the liquid argon calorimeters must be less than  $0.9 E_{\text{c.m.}}$ .

With these stringent cuts, 284 events with 306 three-prong  $\tau$  decays remain. From the theoretical value of the  $\tau$  lifetime, the expected mean  $\tau$  flight distance at 14.5 GeV/c can be calculated and is found to be 0.7 mm. This value is smaller than the expected resolution (3-4 mm) of the decay vertex, and hence the measurement of the lifetime requires statistical averaging and a good control of systematic errors to achieve the necessary precision.

To improve the quality of the track fits and reduce the contributions of track scattering or mismeasurement, each track in a 3 track jet must have at least ten drift chamber layers, a  $\chi^2$  of less than 40, a distance of closest approach to the beam crossing point of less than 5 mm, and a momentum greater than 500 MeV/c. All tracks must appear to originate from a common point along the incident beam directions with an error of 5 cm. The remaining sample contains 126 three-prong  $\tau$  decays.

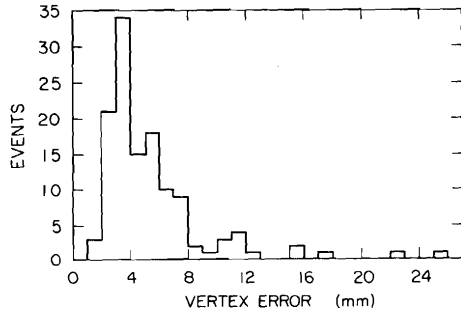


Fig. 25. Vertex resolution along the direction of  $\tau$  flight path.

The vertex resolution along the  $\tau$  direction of flight is shown in fig. 25. The data are divided into two samples, one with vertex uncertainties less than 4 mm, and one with vertex uncertainties between 4 and 8 mm. The 16 events with greater than 8 mm uncertainty and 8 events with poor vertex  $\chi^2$  contain negligible information on the  $\tau$  lifetime and are not used further.

The  $\tau$  flight distance was calculated as the distance between the decay vertex and the beam crossing point. The location of the crossing point was determined by measuring the intersection point of Bhabha events. This position is found to be very stable from run to run at PEP. The observed rms beam spreads were found to be 0.30 mm in the vertical and 0.76 mm in the horizontal. These values are consistent with the experimental resolution and the horizontal beam size respectively.

The  $\tau$  flight distance for all data with vertex uncertainties less than 8mm and for the high resolution sample are shown in fig. 26. In the full sample, one can already see evidence of a nonzero  $\tau$  lifetime. There are 35 events with negative flight distances and 67 events with positive flight distances. The binomial probability that this could come from a distribution with mean zero is about 0.2%. The lifetime is derived from the flight path distributions by doing a maximum likelihood fit to a shape which is determined by the convolution of the vertex resolution function with an exponential decay distribution. The simulation of the vertex resolution includes Coulomb and nuclear scattering which contribute a flat distribution in the region of large flight distances. The result for the mean flight distance is  $1.07 \pm 0.37$  mm where the error is statistical only.

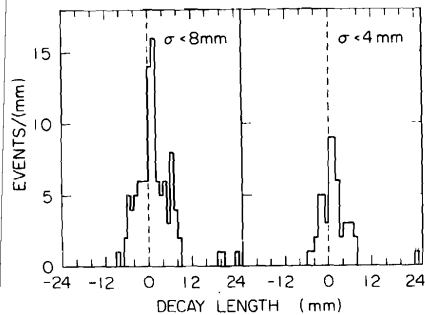


Fig. 26. Distribution of  $\tau$  flight distances at  $\sqrt{s} = 29$  GeV for events with vertex uncertainties less than: (a) 8 mm and (b) 4 mm.

of 7.5 events results in an upward correction of 4% to the mean flight distance. The final result for the  $\tau$  lifetime is

$$\tau_{\tau} = (4.6 \pm 1.9) 10^{-13} \text{ sec.}$$

This is the first nonzero measurement of this quantity.<sup>7</sup> With it we begin to be able to test  $\tau$ - $\mu$  universality and place limits on the weak couplings of the  $\tau$ . Modifications are being made to the MARK II detector to increase the sensitivity of these measurements. The trigger chamber was removed during the summer 1981 shutdown and was replaced with a vertex chamber which should increase the overall vertex resolution by about a factor of three. This together with the improved luminosity of PEP using the minibeta scheme should substantially reduce the errors on the  $\tau$  lifetime and make it possible to begin looking at charmed meson lifetimes.

#### SCALING VIOLATION IN INCLUSIVE HADRON PRODUCTION

At sufficiently high energies, we would expect that all mass scales such as particle masses or quark masses should become unimportant. Hence in simple quark-parton models, the quark fragmentation functions depend only on the initial quark flavor and the dimensionless ratio of the particle energy to the initial quark energy. This "scaling" of the fragmentation function, i.e., dependence only on

$$x = \frac{2E}{\sqrt{s}},$$

leads to a total hadronic cross section in  $e^+e^-$  annihilation which falls as  $1/s$  and a particle energy distribution

$$s \frac{d\sigma}{dx}$$

which is independent of the center of mass energy  $\sqrt{s}$ .

In models with gluon production (QCD) however, the emission of gluons by initial quarks leads to a depletion of the energy available to high energy (or high  $x$ ) hadrons. The presence of a scale parameter  $\Lambda$  in QCD theories leads to a scale in the coupling constant of the quark and gluon and the  $Q^2$  variation of this coupling will destroy the scaling behavior of  $s d\sigma/dx$ . Since the coupling constant varies only logarithmically with  $Q^2$ , these effects are small and require a large range in  $Q^2$  for their detection.

The MARK II detector has collected data both at the SPEAR storage ring and the PEP storage ring and thus has available the inclusive distributions over a large range of  $Q^2$  from  $s = 25 \text{ GeV}^2$  at SPEAR to  $s = 841 \text{ GeV}^2$  at PEP. Many of the difficulties inherent in detecting scaling violations involve the energy dependent corrections for the detection efficiency. By using the same detector in

both energy ranges, the systematic effects that obscure the detection of the  $s$  dependence in  $s d\sigma/dx$  can be reduced.

To measure the inclusive momentum distribution, one must select hadronic events and remove contributions from two-photon interactions,  $\tau$  lepton production, and possible QED or beam-gas backgrounds. The observed sample must be corrected for detection efficiency and radiative effects. In the MARK II detector, the principal event selection criteria are a minimum number of charged particles and a minimum total energy deposit. At SPEAR energies, three or more charged particles are required with a minimum momentum of 100 MeV each. At PEP, five or more particles are required, and the charged energy must be greater than  $0.25 E_{c.m.}$  or greater than 3 GeV when there is at least 4 GeV deposited in photons. Residual backgrounds are determined by Monte Carlo calculation. Decay products from the  $\tau$  lepton and tracks from two-photon events are found to be 3% of all hadronic tracks at 5 GeV and a negligible fraction at PEP energies with these cuts. Beam-gas and beam-wall interactions are eliminated by the requirements that the event vertex lie within 4 cm of the beam axis and 10 cm of the collision point at both energies. Contamination from these events can be measured by using events which originate from 10 cm to 15 cm from the collision point and is found to be 2% at 5 GeV and again negligible at PEP energies. The remaining sample of hadronic tracks consists of 12,000 tracks from 3000 events at 5 GeV and 50,000 tracks from 4500 events at 29 GeV so that statistical errors are very small.

The detection efficiency as a function of  $x$  is calculated with a model (Ali Monte Carlo)<sup>8</sup> which has been adjusted to agree with the observed multiplicity and sphericity distributions. The detection efficiency relates the observed  $x$  distribution to that which would be produced in the absence of radiative effects by including initial state radiation in the Monte Carlo. At 5 GeV, this efficiency falls by approximately a factor of 4 in going from  $x$  of .2 to .8, and at PEP it is nearly constant.

Modifications of the Monte Carlo can be used to estimate the systematic uncertainty in this efficiency. At high energies, the uncertainty is estimated to be  $\pm 10\%$  independent of  $x$  between 0.2 and 0.8. At low energies the uncertainty is approximately  $\pm 15\%$  and may have a slight  $x$  dependence. Additional systematic errors due to background subtractions and normalization uncertainties are 6% at 29 GeV and 8% at 5 GeV.

The results obtained by the MARK II collaboration at 5.2 GeV are compared to those of the MARK I<sup>9</sup> collaboration at 7.4 GeV in fig. 27.

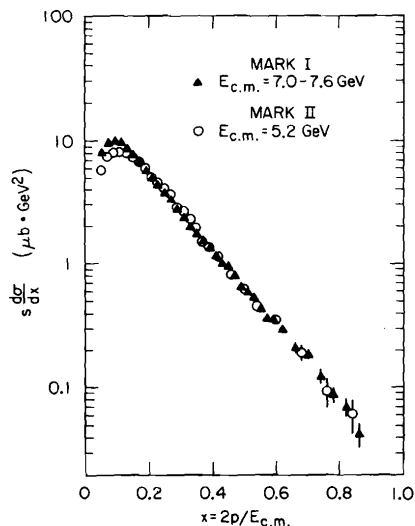


Fig. 27.  $s d\sigma/dx$  from MARK II at 5.2 GeV and from MARK I at 7.4 GeV.

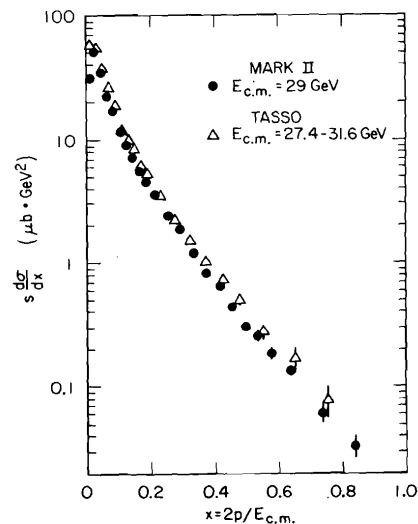


Fig. 28.  $s d\sigma/dx$  from MARK II at 29 GeV and TASSO between 27.4 and 31.6 GeV.

The MARK I collaboration<sup>9</sup> used different cuts and different Monte Carlo models, but the results are in excellent agreement. At low  $x$ , the results are not expected to agree because of the nonscaling behavior introduced by particle masses. This effect should persist up to

$$x \sim \frac{2M}{\sqrt{s}}$$

The high energy results of the MARK II at 29 GeV are compared to those of the TASSO collaboration between 27.4 and 31.6 GeV<sup>10</sup> in fig. 28. Here again there is excellent agreement between the two experiments within the quoted systematic errors. Figure 29 compares the low and high energy data taken by the MARK II collaboration. The high energy data lie below the low energy data throughout the region of  $x$  from .2 to .6 giving clear evidence for an  $s$  dependence of  $s d\sigma/dx$  well outside the expected systematic uncertainty and in violation of scaling behavior.

If scaling were valid, then one would expect that  $s d\sigma/dx$  would be constant as a function of  $s$  for a fixed  $x$  bin. Figure 30 shows that the cross section is in fact falling at high  $s$  and  $x$ . The data is taken from the MARK I, MARK II, and TASSO collaborations. The rise at low  $s$  and low  $x$  is due to the mass effect mentioned previously. A quantitative interpretation of this behavior using Altarelli-Parisi evolution equations<sup>11</sup> is complicated by the lack of knowledge of the charmed quark fragmentation function. Qualitatively, however, the result agrees with the QCD expectation of a depletion of the cross section at high  $x$  which increases with  $s$ .

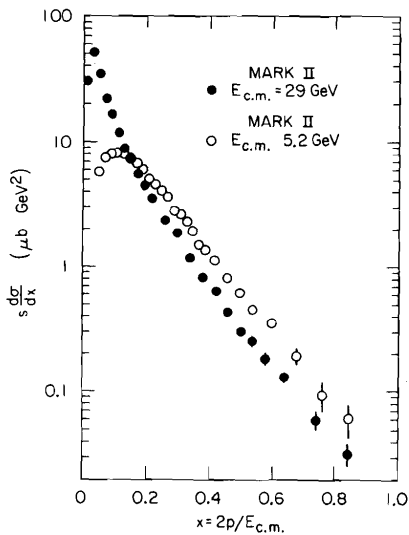


Fig. 29.  $s d\sigma/dx$  from MARK II at low and high energies.

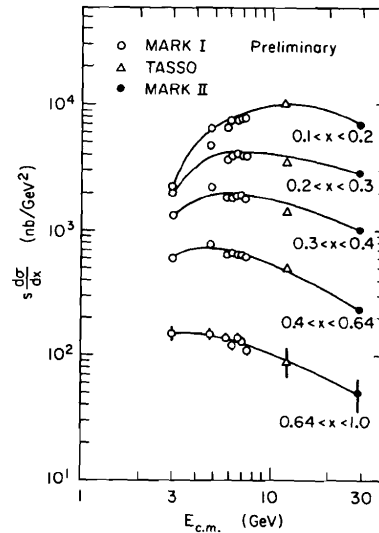


Fig. 30.  $s d\sigma/dx$  versus  $s$  for fixed  $x$  bins from MARK I, TASSO, and MARK II.

#### ENERGY-ENERGY CORRELATIONS

The annihilation of high energy electrons and positrons into multiparticle final states has in recent years become a fruitful testing ground for models of the strong interactions of quarks. The behavior of the total cross section with energy exhibits an energy dependence which is

$$\sigma_{\text{hadrons}}(s) \sim \frac{1}{s}$$

and is therefore characteristic of pointlike particle production. The magnitude of this cross section allows us to calculate the total number of contributing pointlike constituents and the observation of thresholds and bound states has

given us increased confidence that the hadrons are products of a pointlike coupling of the photon to quark antiquark pairs. The subsequent observation of two-jet behavior in the distribution of particles within these multihadron final states allows us to study in detail the way in which these initial quarks fragment into hadrons.<sup>9</sup> The basic features of the data are well described by the quark-parton model.

The attempt to understand the interaction of quarks has led to the proposal of a theory in which the quarks interact via the exchange of massless colored objects called gluons. This exchange is one of the basic ingredients in the theory of Quantum-Chromo-Dynamics or QCD. A second very basic ingredient due to the non-Abelian nature of this theory is the coupling of a gluon to two other gluons. Available energies for electron-positron annihilation have now reached an energy where the effects of gluons or at least the effect of interactions between the quarks have become testable.

One consequence of the presence of gluons in a theory is the appearance of gluon radiation from the initial quarks when the energy becomes high enough. This leads to deviations from the two jet behavior seen at lower energies. This mechanism is now the accepted explanation for a gradual broadening in momentum space of the two jets as the energy increases. It also explains the presence in the data of events with distinctly three jet structure where the three jets tend to lie in a plane as would be expected from a massless radiative process.<sup>12</sup>

Precise tests of QCD have so far relied heavily on Monte Carlo's which parameterize the low energy behavior of  $e^+e^-$  annihilation and quark fragmentation. This behavior is then combined with the effects of gluons as calculated in perturbation theory and the high energy data is compared to the Monte Carlo results with and without the inclusion of the perturbative QCD effects. Uncertainties arise in the parameterization of gluon fragmentation functions (not seen at low energies), heavy quark mass effects, and nonperturbative contributions to the fragmentation. In many cases it is difficult to separate the genuine properties of QCD from the dependence of the Monte Carlo models on the details of the fragmentation process.

To test QCD in a clean way it is preferable to find quantities which are insensitive to the fragmentation process and which are still calculable within the framework of the theory. In QCD it is important to choose an observable which is insensitive to the presence of soft gluons or the presence of gluons which are collinear or anticollinear with a quark. This is because the theory is singular in all of these cases.

The question of finding observables which are insensitive to these problems and also insensitive to the fragmentation process has been examined by several authors.<sup>13-14</sup> In particular, Basham, Brown, Ellis, and Love have described a hierarchy of observables which appear to have the desired properties. The simplest cross section theoretically is the total annihilation cross section or the ratio

$$R = \frac{\sigma}{\sigma_{\mu\mu}} .$$

However, the experimental uncertainties in this measurement are unfortunately larger at the moment than the predicted QCD effect. The second simplest measurement is the energy weighted angular distribution or "antenna" pattern of the produced hadrons. In this case, the energy weighting eliminates the singularity due to soft gluon emission. Furthermore, since the energy is carried by hadrons and these are included regardless of whether they come from a gluon or quark, the remaining singularities due to collinear quark-gluon branchings are also eliminated.<sup>15</sup>

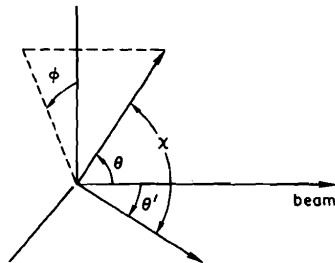


Fig. 31. Definition of the angles used for Energy-Energy correlation measurements.

The main features of the antenna pattern are the two lobes of energy due to the production of two jets from the initial quark-antiquark pair. The minima between the lobes are sensitive to the gluon radiation pattern and become filled in with an energy dependence which is  $\ln \sqrt{s}$ . However, these minima are also filled in by the quark fragmentation process with an energy dependence  $1/\sqrt{s}$ . Untangling the two effects is difficult.

The double energy cross section<sup>16</sup> requires the measurement of the angular distribution and correla-

ions of two energy deposits  $dE$  and  $dE'$  into solid angles  $d\Omega$  and  $d\Omega'$ . The two elements of solid angle are specified by four angles  $(\theta, \phi, \theta', \phi')$  as shown in Fig. 31. As a function of the angle  $\chi$  between  $d\Omega$  and  $d\Omega'$ , the cross section can be written as the sum of a QCD contribution and a correction for quark fragmentation and heavy lepton decay.

$$\frac{1}{\sigma} \frac{d^2\Sigma}{d\Omega d\Omega'} = \mathcal{A}^{\text{QCD}}(\chi) \frac{1}{\sigma} \left( \frac{d\sigma}{d\Omega} + \frac{d\sigma}{d\Omega'} \right) + \mathcal{B}(\chi) \frac{3}{16\pi} (\cos\chi + \cos\theta\cos\theta') \\ + \mathcal{A}^{\text{qf}}(\chi) \frac{1}{\sigma} \left( \frac{d\sigma}{d\Omega} + \frac{d\sigma}{d\Omega'} \right) + \mathcal{A}^{\text{H.L.}}(\chi) \frac{1}{\sigma} \left( \frac{d\sigma}{d\Omega} + \frac{d\sigma}{d\Omega'} \right) .$$

The coefficients  $\mathcal{A}$  and  $\mathcal{B}$  can be calculated. The first order perturbation result in QCD yields

$$\mathcal{A}^{\text{QCD}}(\chi) = \frac{\alpha_s}{12\pi} \frac{1}{1-z} \left[ \left( \frac{3}{z^5} - \frac{4}{z^4} \right) \ln(1-z) + \frac{3}{z^4} - \frac{5}{2z^3} - \frac{1}{z^2} \right] \\ \mathcal{B}^{\text{QCD}}(\chi) = \frac{\alpha_s}{12\pi} \frac{1}{1-z} \left[ \left( \frac{12}{z^5} - \frac{16}{z^4} + \frac{4}{z^3} \right) \ln(1-z) + \frac{12}{z^4} - \frac{10}{z^3} \right]$$

where  $z = \frac{1}{2}(1 - \cos\chi)$ . The quark fragmentation and heavy lepton contributions are

$$\mathcal{A}^{\text{qf}}(\chi) = \frac{C \langle p_T \rangle}{4\pi\sqrt{s}} \sin^{-3}\chi \\ \mathcal{A}^{\text{H.L.}}(\chi) = \text{constant} \times \left[ \frac{1}{(1 - v\cos\chi)^3} + \frac{1}{(1 + v\cos\chi)^3} \right]$$

where the constant  $C$  is determined by the multiplicity growth, i.e.

$$\langle n_{\text{tot}} \rangle = C \ln \sqrt{s} + \text{constant} .$$

The most interesting feature of this cross section is that the contribution from quark fragmentation and lepton decay is symmetric under the exchange  $\chi \rightarrow \pi - \chi$  while both QCD contributions are asymmetric. Thus by considering only the cross section

$$\mathcal{D}(\chi) = \frac{d\Sigma}{d\cos\chi}(\pi - \chi) - \frac{d\Sigma}{d\cos\chi}(\chi) ,$$

the quark fragmentation and heavy lepton decay contributions can be eliminated. The experimental analysis of this cross section is done by using

$$\frac{1}{\sigma} \frac{d\Sigma}{d\Omega d\Omega'} = \frac{S_N}{N} \sum_{\text{N events}} \sum_{i,j} \frac{E_i}{\sqrt{s}} \frac{E_j}{\sqrt{s}}$$

where the first sum is over all events and the second is over all pairs of particles. The statistical factor  $S_N$  is one for  $i = j$  and two for  $i \neq j$ . The normalization is found by energy conservation to be

$$\frac{1}{\sigma} \int \frac{d\Sigma}{d\Omega d\Omega'} d\Omega d\Omega' = 1$$

The analysis is done with a sample of  $15,000 \text{ nb}^{-1}$  taken at 29 GeV by the MARK II collaboration. Events are accepted if there are at least five charged tracks and the total visible energy (charged + photons) is greater than 15 GeV. Good charged tracks must have momenta greater than 100 MeV/c and photons must have an energy of at least 200 MeV. Photons which share more than 50% of their energy with another track or which are closer than 10 cm to a charged track at the entrance to the liquid argon barrel are not used. The fiducial volume is  $0.72 < \theta < \pi - 0.72$  in the polar angle and 87% of  $2\pi$  in the azimuthal angle due to eight gaps of  $6^\circ$  at the edges of the liquid argon modules. This leaves a total of 3250 events. Corrections for resolution, efficiencies, and initial state radiation are small (5% - 20%) within the solid angle and for a range of  $30^\circ < \chi < 150^\circ$ .

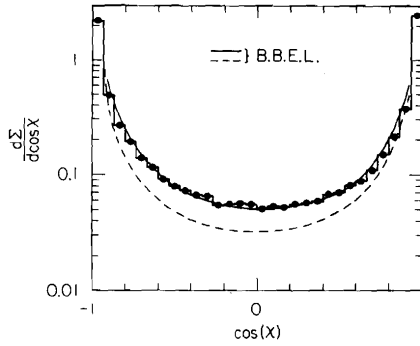


Fig. 32 Energy-Energy Cross-Section versus  $\cos(\chi)$

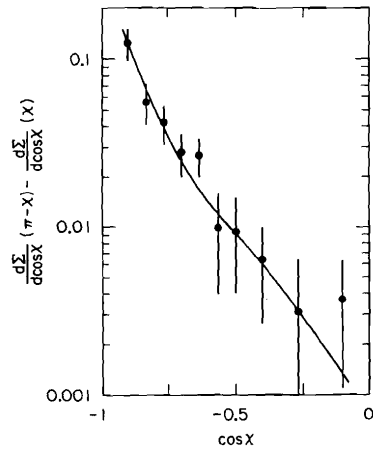
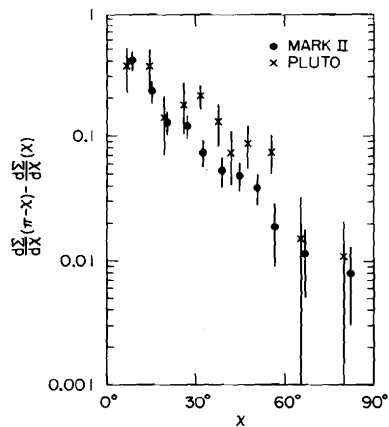


Fig. 33. Asymmetry in the Energy-Energy Cross-Section.



The corrected double energy cross section is shown in fig. 32, integrated over all angles except the relative separation  $\chi$ . The QCD prediction shown in this case contains the symmetric contribution from quark fragmentation and the asymmetric gluon contribution as predicted by the Ali Monte Carlo. The sensitivity to QCD effects is illustrated by the lower curve which is obtained from the same Monte Carlo with  $\alpha_s = 0$ .

As discussed previously, a much cleaner test of QCD is obtained by using the Monte Carlo only to calculate efficiencies and acceptance calculations and then comparing to an observable such as  $\mathcal{D}(\chi)$  which is insensitive to quark fragmentation. The measured values of  $\mathcal{D}(\chi)$  are shown in fig. 33. They vary by almost two orders of magnitude between  $\chi = 30^\circ$  and  $\chi = 90^\circ$ , a range for which we expect the perturbative calculation of Basham, Brown, Ellis, and Love to be valid.  $\mathcal{D}(\chi)$  would of course be zero if there were no QCD effects. The shape of  $\mathcal{D}(\chi)$  is completely determined by the perturbative QCD calculation with the normalization fixed by the value of  $\alpha_s$ . Fitting this normalization yields

$$\alpha_s = 0.18 \pm 0.015 \pm 0.03$$

This agrees well with a similar determination by the PLUTO group using charged particles only. They obtain<sup>17</sup> (see fig. 34)

$$\alpha_s = 0.20 \pm 0.02$$

The detailed agreement of the perturbative calculation with the data is encouraging. The value of  $\alpha_s$  obtained above will be modified by higher order corrections as they become available. It will not be necessary to modify the measured values of  $\mathcal{D}(\chi)$  however since they depend on the Monte Carlo only to determine the efficiencies.

In summary, this measurement is relatively independent of the theory, it is insensitive to details of the fragmentation model, it uses all events (not just 3-jet events) without having to use an event-by-event axis determination, and finally there exists a theoretical prediction which agrees well in shape with the data and whose normalization determines the coupling constant  $\alpha_s$ .

#### SINGLE JET ENERGY MOMENTS

In the previous section, the wide angle asymmetry in energy-energy correlations was shown to be sensitive to gluon radiation and calculable within the framework of QCD. That calculation uses a perturbative approach to calculate this one hard gluon process. The quark fragmentation process which involves multiple soft gluon branchings and leads to the formation of quark jets is not calculated in the approach of Basham, Brown, Ellis and Love. Instead, the observation of jets with a  $p_{\perp}$  cut-off and the measured behavior of multiplicity with energy is used to parameterize the quark

Fig. 34. Comparison of the Energy-Energy Asymmetry measured by MARK II (charged and neutrals) and PLUTO (charged).

fragmentation as

$$\frac{1}{\sigma} \frac{d^2 \Sigma}{d\Omega d\Omega'} = \frac{C \langle p_{\perp} \rangle}{4\pi\sqrt{s}} \sin^{-3} \chi \frac{1}{\sigma} \left( \frac{d\sigma}{d\Omega} + \frac{d\sigma}{d\Omega'} \right)$$

where

$$\langle N_{\text{tot}} \rangle = C \ln \sqrt{s} + \text{constant}$$

It is quite natural to wonder at this point whether this limited  $p_{\perp}$  behavior can be derived from the properties of QCD. Some progress in this direction has been made. Since the quark fragmentation process involves multiple soft gluon emission, the calculations are done in a leading log formulation. Sterman and Weinberg<sup>18</sup> showed that the probability for observing all but a fraction  $\epsilon \ll 1$  of the total energy within a pair of back-to-back cones of half angle  $\delta \ll 1$  could be calculated and indicates the formation of jets. Further progress along this same line has been made by Konishi, Ukawa, and Vengiano<sup>19</sup> who have shown that the energy weighted cross-sections of particles within a single jet can be calculated using a "jet calculus" approach.

If one starts with an initial parton  $i$  (quark or gluon), then the jet will develop from a series of branchings indicated schematically in fig. 35. Each branch in the development of this "shower" has a probability which is determined to first order in  $\alpha_s$  by the Altarelli-Parisi functions.<sup>11</sup> In a process which can be characterized by one large scale  $Q^2$ , the probability of beginning with a parton  $i$  and ending with a parton  $j$  with a fraction  $x$  of the initial energy is found by summing over all possible branchings which lead to  $j$  and is effectively described by the parton fragmentation function

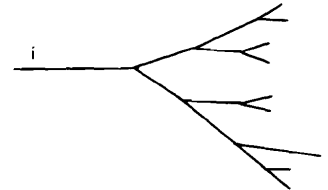
$$D_{ji}(x, Y)$$

where

$$Y = \frac{1}{2\pi b} \log \left[ \frac{\alpha_s(\mu^2)}{\alpha_s(Q^2)} \right]$$

and

$$b = \frac{11N_c - 2N_f}{12\pi}$$



The interest in this formalism is that it has been shown that a certain measurable extension of the Sterman-Weinberg two-jet cross section is simply related to these parton distributions.<sup>20</sup> The single jet cross section for a cone of half angle  $\delta$  satisfies the relation

Fig. 35. Parton shower leading from parton  $i$  to parton  $j$ .

$$\frac{1}{\sigma_i} \frac{d\sigma_i(\delta)}{dx} = \sum_j D_{ji}(x, Y - Y_\delta)$$

where

$$Y_\delta = \frac{1}{2\pi b} \log \frac{\alpha_s(\mu^2)}{\alpha_s(\delta^2 Q^2)}$$

Since this is a function of  $Y - Y_\delta$ , the  $Q^2$  dependence of  $\alpha_s$  enters only in the combination

$$\log \frac{\alpha_s(\delta^2 Q^2)}{\alpha_s(Q^2)}$$

In order to avoid the usual infrared divergence problems, it is again necessary to study energy weighted cross sections. The energy moments are defined by

$$C_n^i(\delta) = \frac{1}{\sigma_i} \int \frac{d\sigma_i(\delta)}{dE} \left( \frac{2E}{\sqrt{Q^2}} \right)^n dE$$

where  $i$  refers to the choice of a quark or gluon jet, and  $n$  is the order of the moment. By substituting in the relation given above between the cross section and the  $D_{ji}$ , and using the known  $Q^2$  evolution of the parton fragmentation functions, one finds a system of coupled differential equations for  $C_n^q(\delta, Q^2)$  and  $C_n^g(\delta, Q^2)$  in terms of the anomalous dimension matrix

$$(A_n)_{ji} = \int_0^1 dz z^n P_{ji}(z)$$

where the  $P_{ji}$  are the Altarelli-Parisi functions. These equations can be solved and the result is

$$C_n^i(\delta, Q^2) = \alpha_n^i \left( \frac{\alpha_s(\delta^2 Q^2)}{\alpha_s(Q^2)} \right)^{\lambda_n^+/2\pi b} + \beta_n^i \left( \frac{\alpha_s(\delta^2 Q^2)}{\alpha_s(Q^2)} \right)^{\lambda_n^-/2\pi b}$$

where  $\lambda_n^+$ ,  $\lambda_n^-$  are the eigenvalues of  $A_n$  and the  $\alpha_n^i$ ,  $\beta_n^i$  are the quark or gluon components of the eigenvectors belonging to  $\lambda_n^+$  and  $\lambda_n^-$ . These solutions provide an absolutely normalized prediction for the moments which can be used to test QCD. For example, the second moment for the choice  $N_c = 3$ ,  $N_f = 4$  is given by

$$C_2(\delta, Q^2) = 1.1653 \left( \frac{\alpha_s(\delta^2 Q^2)}{\alpha_s(Q^2)} \right)^{-0.6085} - 0.1653 \left( \frac{\alpha_s(\delta^2 Q^2)}{\alpha_s(Q^2)} \right)^{-1.386}$$

That there is a connection between the cone angle  $\delta$  and the virtual mass  $q^2$  of a parton can be understood in first order perturbation theory by considering the decay of a parton with energy  $x$  which decays into two other partons with opening angle  $2\delta$ . From fig. 36 we can see that the  $q^2$  is given by

$$q^2 = x^2(1-z)z Q^2 \sin^2 \delta .$$

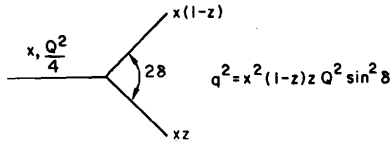


Fig. 36. First order diagram relation between momentum transfer  $q^2$  and angle  $\delta$ .

Here  $q^2$  is the on-shell mass of the initial parton. Integrating over all branching processes which lead to an off-shell mass  $\sqrt{q^2}$  where the decay products are restricted to lie within a cone has been shown to be equivalent to the choice of a parton with on-shell mass  $\sqrt{q^2}$ .<sup>4</sup> This on shell mass then determines the maximum transverse momentum spread of the decay products via the relation given above.

One way of testing QCD would be to look for jet broadening as a function of  $Q^2$ . One could for example measure a Sterman-Weinberg cross section with fixed angle  $\delta$  for various values of beam energy or  $Q^2$ . The method proposed here is to instead look at the variation of the cross section with  $\delta$  at a fixed  $Q^2$ . Experimentally one cannot measure the values of the energy fractions  $z$ ,  $(1-z)$  of the decay products or the  $x$  of the initial parton. Instead one observes a fractional energy  $x'$  deposited within the cone of opening angle  $2\delta$ . A reasonable approximation is then

$$x^2 z(1-z) \approx \frac{1}{4} x'^2$$

and the mass formula becomes

$$4q^2 = x'^2 Q^2 \sin^2 \delta .$$

For each jet, the energy moments are found by measuring the energy flow  $E_i$  into cones with fixed opening angle  $2\delta$  and forming the sum

$$C_n(\delta) = \sum \left( \frac{E_i}{E_{vis}} \right)^n .$$

The mean value of  $x'$  for this jet is given by

$$x' = \frac{1}{N_j} \sum_{i=1}^{N_j} \frac{E_i}{\sum_{i=1}^{N_j} E_i} = \frac{1}{N_j}$$

Finally, the mean values of  $x'$  and  $C_n$  are calculated from an average over all accepted jets.

This analysis has been carried out with the MARK II detector. Since the MARK II measures both charged and neutral particles, the scheme for dividing the detector into cones of opening angle  $2\delta$  can be defined entirely by the analysis program. These software calorimeters are defined by dividing the polar angle range  $10^\circ < \theta < 170^\circ$  into equal  $\Delta\theta$  bins. For each central value  $\theta_0$ , the azimuthal angles are divided into  $\Delta\phi$  bins in such a way that the solid angle is the same for all  $\theta_0$ . The angle  $\delta$  is calculated by determining the cone with opening angle  $2\delta$  which would have this same solid angle.

For a given event, different values of  $x'$  and  $C_n(\delta)$  would be obtained for different orientations of the jet axis with respect to the calorimeter centers. For definiteness, we always rotate the calorimeters so that the jet axis determined from the sum of all neutral and charged momenta points to the center of a calorimeter. This in effect maximizes the value of  $\langle x' \rangle$ . The energies  $E_i$  for neutrals are calculated from the measured photon energies. Charged particles are assumed to be pions except for those which have been identified as  $e$ ,  $\mu$ ,  $K$ , or  $p$ . Kaon identification extends to 1.4 GeV/c and proton identification to 2 GeV/c. No attempt is made to reconstruct neutral kaons or pions. This leads to a restriction that we cannot interpret the results for

$$q^2 \lesssim \left( \frac{M_{K,\pi,p}}{2} \right)^2$$

since at this low a  $q^2$ , the transverse development of the parton shower is determined by the hadron masses. This restriction is equivalent to the restriction

$$q^2 \ll \Lambda^2$$

which specifies the point at which nonperturbative effects will dominate. Both say that one cannot interpret the results if the angle  $\delta$  is too small.

The data used for this analysis is the sample of 29 GeV data taken by the MARK II since January 1981 (15,400 nb<sup>-1</sup>). The polar angle fiducial volume is  $50^\circ < \theta < 130^\circ$ . Charged tracks are required to have at least 100 MeV/c momentum, and photons must have a measured energy greater than 300 MeV. Photons which are closer than 15 cm to a charged track at the entrance to the liquid argon shower counters are discarded. Each event is analyzed as a two-jet event and the thrust axis is required to fall between  $65^\circ$  and  $115^\circ$  in the polar angle to ensure that most of the jet energy falls within the solid angle. In addition, each jet must have at least 8 GeV and must contain at least 2 charged particles and at least one other particle charged or neutral. The event must have a charged multiplicity of at least five to discriminate against  $\tau$  pair production, and events containing an electron with  $E > 8$  GeV are discarded to eliminate showering Bhabhas. Finally, the thrust of the event has to be greater than .85. This cut results from the fact that the jet calculus calculations require that there be only one large  $Q^2$  in the process. Three jet events then must be eliminated since they represent the radiation of hard gluons.

The measured values of  $C_n(\delta)$  and  $\langle x' \rangle$  have been corrected for the effects of jet selection, undetected energy, initial state radiation,  $\tau$  pair contamination, and the weak decays of charmed and bottom mesons. The correction factors are determined by comparing the analysis of Monte Carlo events with all of the above effects included with the results of the same analysis for an ideal detector, no initial state radiation, no event cuts except the thrust cut and no produced  $\tau$ 's or heavy mesons. This correction procedure is not very sensitive to the details of the Monte Carlo. The ratio of generated pseudoscalar to vector particles was varied between 1:1 and 3:1 and the light quark fragmentation parameter  $a$  was varied from 0.50 to 0.70. The resulting corrections are indistinguishable within the errors.

The values chosen for the cone half-angles for this analysis were  $13.06^\circ$ ,  $18.26^\circ$ ,  $23.32^\circ$ ,  $29.50^\circ$ , and  $47.80^\circ$ . For comparison, the typical size of a jet

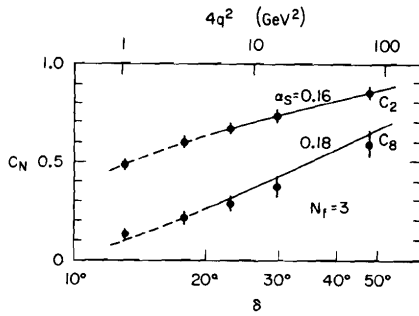


Fig. 37.  $C_2(\delta)$  and  $C_8(\delta)$  with jet calculus predictions.

previous determinations of  $\alpha_s$  and with the value obtained from the energy-energy correlation method. In addition to using the normalization of the  $C_n$  to determine  $\alpha_s(Q^2) = (29 \text{ GeV})^2$ , we can invert the formulae for the  $C_n$  to obtain the variation of  $\alpha_s$  with  $q^2$ . Using the formula for  $C_n$  in terms of  $\alpha_n, \beta_n, \lambda_n^+$  and  $\lambda_n^-$  we find

$$\frac{\alpha_s(x'2\delta^2Q^2)}{\alpha_s(Q^2)} = f(C_n(\delta)) .$$

The behavior of  $\alpha_s$  deduced from the moment  $C_2$  is shown in fig. 38. Similar plots are obtained from the other moments. The data agree remarkably well with the logarithmic variation predicted by QCD which is shown on the figure for  $N_f = 3$  and  $\alpha_s(29 \text{ GeV}) = 0.16$ . The  $4q^2$  conversion for each  $\delta$  has an estimated systematic

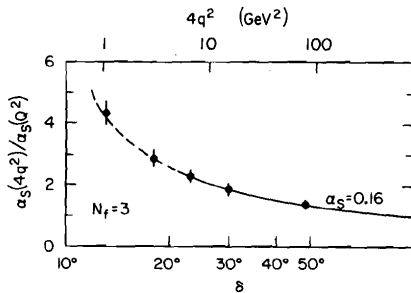


Fig. 38.  $Q^2$  behavior of  $\alpha_s$  deduced from  $C_2(\delta)$ .

at these energies is represented by a half-angle of approximately  $20^\circ$ . The values of  $C_n(\delta)$  for  $n = 2, 8$  are shown in fig. 37. The curves shown are the absolutely normalized predictions of the jet calculus approach where the number of flavors  $N_f$  has been set to three. In principle there are five flavors available, and the number of effective flavors may even be a function of  $q^2$ . Since we have corrected for the effects of heavy meson production, however, one would expect that the choice of three flavors would be more correct. The statistical accuracy of the data does not yet warrant a detailed examination of this point. The theoretical curve for  $N_f = 4$  lies approximately one sigma lower at each point than the  $N_f = 3$  curve for  $C_2$ .

We have found that the value of  $\alpha_s$  at 29 GeV must be varied from  $\alpha_s(29 \text{ GeV}) = 0.16$  to  $\alpha_s(29 \text{ GeV}) = 0.18$  to fit the normalization of  $C_2$  and  $C_8$  respectively. This value agrees well with

uncertainty of 30%. This error is the linear sum of the error due to resolution and statistics in the determination of  $\langle x' \rangle$  and a systematic error for the Monte Carlo correction procedure which is assumed to be 20% of the correction which must be applied to  $\langle x' \rangle$ .

The agreement between the data and the theoretical predictions extends over a surprising range in  $4q^2$ . The lowest value is not much larger than a typical hadronic mass scale and represents a value of  $\alpha_s$  of approximately 0.7! At this large a value of  $\alpha_s$  it is surprising that the leading log approach works as well as it does. The question of where nonperturbative effects begin to dominate in jet physics is not yet settled and perhaps this approach will give us some insight into that question.

### THREE JET PHYSICS

To study the properties of gluon jets, the MARK II collaboration has used a cluster algorithm developed by J. Dorfan<sup>21</sup> to select and analyze a sample of events which have three jet-like behavior. A similar algorithm has been suggested by Daum, Meyer and Burger.<sup>22</sup> The major advantage of these methods is that in contrast to methods like triplicity<sup>23</sup> and trijettiness,<sup>24</sup> they make no initial assumptions about the number of jets in an event and can therefore be applied in an unbiased way to search for 2, 3, 4 or  $n$  jet events.

The particular method used here begins by choosing a metric which defines the "distance" between any two particles with momenta  $p_i$  and  $p_j$ . The particles are then connected by what is known as a minimal spanning tree, i.e., the set of lines which minimizes the total length. Clusters of particles can then be formed by grouping together those particles which are separated by short "distances". This clustering requires only a criteria for defining when a line joining two particles

is too long to be included within a cluster. By adjusting this criteria, one can optimize the algorithm for example to minimize the contamination of two-jet events in the three-jet sample. A different optimum might be required for efficient recognition of four-jet events.

In the analysis which follows, the algorithm has been adjusted using  $q\bar{q}$  and  $q\bar{q}g$  events generated by the Ali Monte Carlo so that the contamination of two-jet events in the three cluster sample is 9%. This is approximately a factor of two smaller contamination than that of methods which assume as a starting point that all events are three-jet-like and then cut on a measure like triplicity. The distribution of clusters found in the data together with the Monte Carlo estimate of the  $q\bar{q}$  contamination is shown in fig. 39.

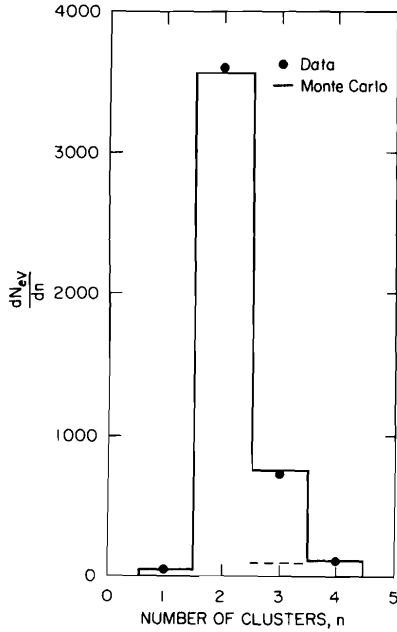


Fig. 39. Cluster distribution in hadronic events with Monte Carlo prediction of  $q\bar{q}$  contamination for 3-cluster events.

The Monte Carlo is also used to find the resolution of this algorithm in reconstructing various properties of the initial three partons in three-jet events. The energies of the partons are calculated from the relative angles of the three momentum vectors defined by summing all the momenta within a cluster. These momenta reproduce the directions of the initial partons to within  $4^\circ$ ,  $6^\circ$  and  $10^\circ$  for the highest, intermediate and lowest energy jets respectively. The resulting resolution in the variable thrust is 6%.

The first property of the three-jet events that has been examined in detail is the question of the gluon spin. The method is to define the fractional energy  $x_i = 2E_i/E_{c.m.}$  of each of the three jets such that

$$x_1 \geq x_2 \geq x_3$$

and

$$\sum x_i = 2$$

The distributions of the  $x_i$  are known in first order QCD<sup>25</sup> to be

$$\frac{1}{\sigma_0} \frac{d\sigma}{dx_1 dx_2} = \frac{2\alpha_s}{3\pi} \left[ \frac{x_1^2 + x_2^2}{(1-x_1)(1-x_2)} + \begin{matrix} (1,2,3) \\ \text{cyclic} \\ \text{permutations} \end{matrix} \right]$$

where  $\sigma_0$  is the two jet cross section. There is no rigorous theory with a spin-zero gluon, but the final state angular distributions can be determined and the cross section is

$$\frac{1}{\sigma_0} \frac{d\sigma}{dx_1 dx_2} = \frac{\tilde{\alpha}_s}{3\pi} \left[ \frac{x_3^2}{(1-x_1)(1-x_2)} + \begin{matrix} \text{cyclic} \\ \text{permutations} \end{matrix} \right]$$

To distinguish between these two distributions, Ellis and Karliner<sup>26</sup> have suggested looking at the angular distribution of  $x_2$  and  $x_3$  relative to  $x_1$  in the center-of-mass frame of  $x_2$  and  $x_3$ . This procedure is illustrated in fig. 40. The angle  $\tilde{\theta}$  is determined from

$$\cos \tilde{\theta} = \frac{x_2 - x_3}{x_1}$$

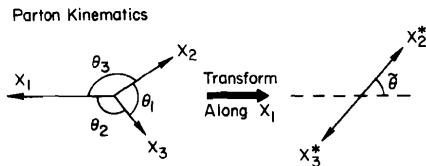


Fig. 40. Ellis-Karliner definition of  $\tilde{\theta}$ .

This analysis was first carried out by the TASSO<sup>27</sup> and PLUTO<sup>28</sup> collaborations.

The predictions of the vector and scalar gluon distributions are shown in figs. 41 and 42. Events where  $x_1$  is greater than 0.9 must be eliminated since the first order cross sections are singular for  $x_1 = 1$ . In addition, the region near  $x_1 = 1$  has a large contamination from two-jet events and the distribution there is dominated by

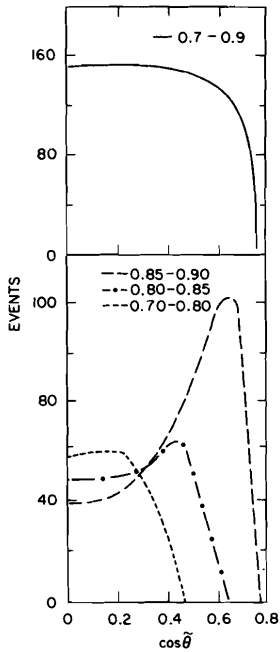


Fig. 41. Vector gluon prediction for the  $\cos\theta$  distribution.

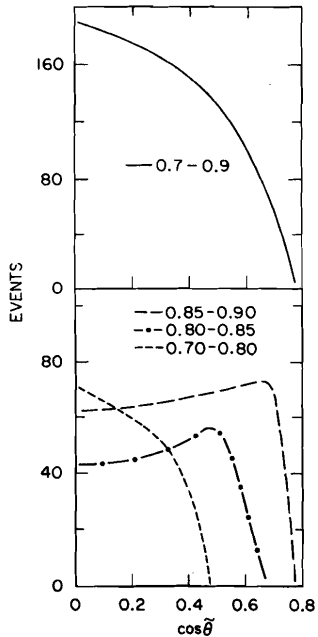


Fig. 42. Scalar gluon prediction for the  $\cos\theta$  distribution.

fragmentation effects and not by gluon emission. Figures 41 and 42 illustrate the two main difficulties in this analysis. The difference between the scalar and vector distributions is largest for small and large values of  $\cos\theta$ . But for small values, the level of the cross section will be sensitive to the maximum value of  $x_1$  which is used and for large values, it will be quite sensitive to the resolution in thrust or  $x_1$ . The measured distribution versus  $\cos\theta$  together with the vector and scalar predictions are shown in fig. 43. Although the vector prediction is a better fit than the scalar prediction, the importance of the first and last bins is clear. Because of the  $x_1$  dependence in this analysis, the MARK II collaboration has determined the average value of  $\cos\theta$  as a function of thrust. This is shown in fig. 44. The data still show a preference for the vector interpretation for values of  $x_1$  between 0.80 and 0.87. At lower values of  $x_1$ , there is no difference between the predicted values of the two theories, and at higher values there may be large systematic problems in both the theory and the measurement.

It is also interesting to investigate the possible differences in fragmentation properties of gluon and quark jets. Gluon jets are expected to have larger multiplicities and larger  $\langle p_{\perp} \rangle$  values than quark jets of the same energy. Since the lowest energy jet in a three-jet event contains the gluon approximately 50% of the time, one could compare the properties of the lowest jet with those of the intermediate and highest energy jets. This would be

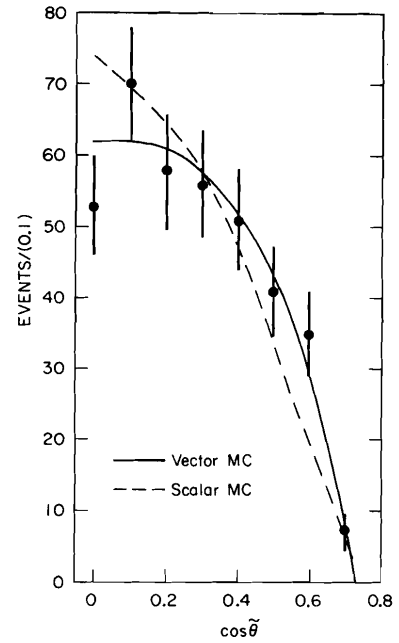


Fig. 43. Detected events versus  $\cos\theta$  with vector and scalar gluon predictions.

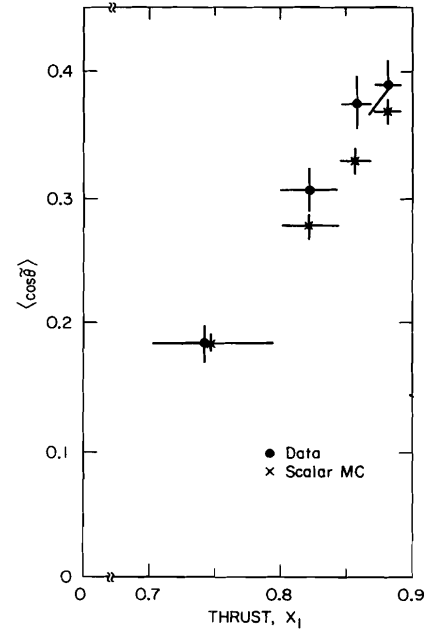


Fig. 44. Average value of  $\cos\theta$  versus thrust.

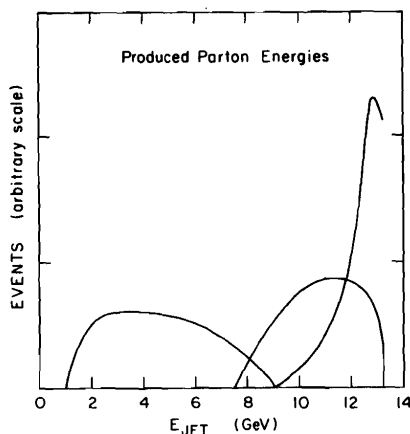


Fig. 45. Produced energy distributions for initial partons in 3-jet events.

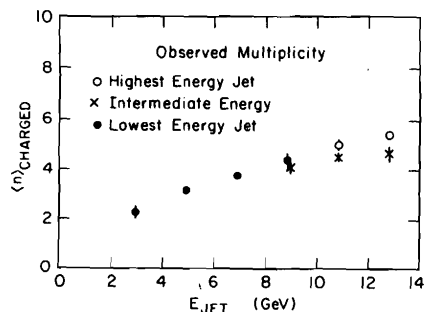


Fig. 46. Uncorrected  $\langle n_{CH} \rangle$  versus jet energy calculated from the jet angles.

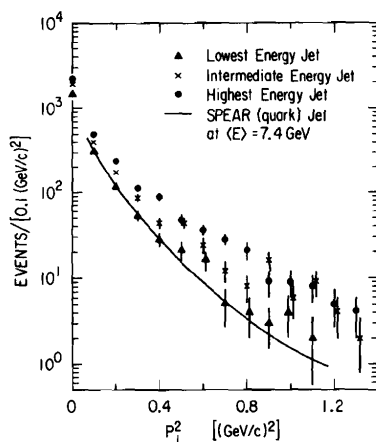


Fig. 47. Comparison of the lowest energy jet  $P_{\perp}^2$  with quark jet distribution at the same average energy.

incorrect however because it would be comparing jets of different average energies, and it is known from low energy data that jet properties like multiplicity are energy dependent. This difficulty is compounded by the fact that there is little overlap between the produced energies of the three partons in a three-jet event. The produced energy distributions are shown in fig. 45 for  $E_{c.m.} = 29$  GeV. There is only a small region where the lowest energy jet and the intermediate energy jet overlap. The overlap between the intermediate and highest energy jets is larger, but the gluon fraction in the intermediate jet is small.

To illustrate the difficulties of isolating gluon fragmentation properties from quark properties, fig. 46 shows the uncorrected average multiplicity of the low, intermediate and high energy jets as a function of the energy calculated from the jet angles. In the region of overlap between the low and intermediate jets there is not yet a significant difference in multiplicity. At the highest energies, there is a trend for the intermediate jet multiplicity to be lower than that of the highest energy jet. This is opposite of what one would expect in QCD since the intermediate jet has a higher gluon content. This effect can probably be understood in terms of the bias which is introduced by the formation of the lowest energy jet. When the intermediate jet has high energy, the lowest energy jet must be very soft. In order to recognize it as a separate jet, it must "steal" particles from one of the other two jets, and these particles will come preferentially from the intermediate jet. A test of gluon fragmentation will require correction for these observation biases.

The properties of gluons can also be investigated by comparing the distributions obtained for the lowest energy jet in a three-jet event with those obtained for quark jets at lower energies. From fig. 45 it can be seen that the average energy of the lowest energy jet is close to the energy available to quark jets at the top of the SPEAR energy range. Figure 47 shows the distribution in  $p_{\perp}^2$  for the three jets at high energy. The lowest energy jet has a shape which is the same as that obtained at low energies by the MARK I collaboration for quark jets. This indicates that the gluon fragmentation function is qualitatively similar to the quark fragmentation function at these energies.

#### PHYSICS WITH $K_s, p, \Lambda$

As we learn more and more about the fragmentation of quarks and gluons into hadrons, we would eventually like to understand the detailed mechanisms involved. There are two issues here. First, we would like to see the differences between the fragmentation of gluon jets and quark jets, and also the differences between the fragmentation of the different flavors of jets (charmed, bottom, strange, etc.). The second issue is that we would like to understand the constraints imposed by the conservation of strangeness, charm, baryon number and charge in the hope that this could discriminate between various dynamical models. As discussed previously, we are

just beginning the investigation of the relative properties of gluon and quark jets using the softest jet in a three-jet event as an enriched sample of gluon jets. Unfortunately, we cannot yet separate out a sample of events which are charmed jets, or strange jets or bottom jets. Instead, however, we can begin this study by looking for strange mesons and baryons within jets. Some of these particles will come of course from pairs of strange mesons or pairs of baryons produced in the fragmentation process itself and hence we will learn about the dynamics of fragmentation but not about the properties of strange quark induced jets. Eventually, leading strange mesons or charmed mesons may help to flavor tag jets and leading baryons may give clues about baryon conservation within jets.

### $K_S$ mesons

From the data taken at 29 GeV, the Mark II collaboration has a sample of 583  $\pi^+\pi^-$  pairs observed within the  $K_S$  mass region ( $475 < M_{\pi\pi} < 525$  MeV/c<sup>2</sup>) with a background of 166 found from side bands 50 MeV away. The observed  $\pi\pi$  invariant mass distribution is shown in fig. 48. The advantage of using  $K_S$  rather than charged K's is that they can be detected with reasonable efficiency over a large range in momentum. The efficiency of the cuts to be discussed below is shown in fig. 49.

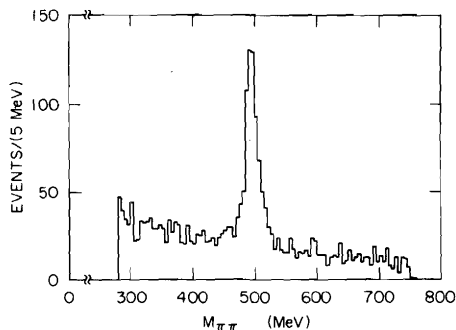


Fig. 48.  $\pi\pi$  invariant mass distribution for  $K_S$  selection.

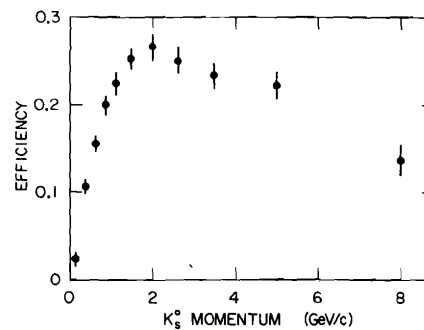


Fig. 49.  $K_S$  efficiency versus momentum.

Since like the pions, the K's are mostly produced at low momenta, the average efficiency is near 0.15. It varies slowly and reaches 0.14 at 8 GeV/c.

The event cuts used in this analysis are the same as those used in the analysis of the charged particle inclusive spectra in order to facilitate the comparison of the properties of the K's with the properties of all charged particles. Each particle of a selected  $\pi^+\pi^-$  pair is required to have a distance of closest approach to the beam crossing point in the xy plane of greater than 0.25 cm. The relative separation of the two tracks in the longitudinal direction at this point must be less than 20 cm. The information from the time-of-flight system for each track is required to be consistent with the interpretation that is a  $\pi$  meson. The decay vertex is found from the crossing point of the two tracks and the momentum vector of the  $K_S$  at this point is required to have a distance of closest approach of less than 0.5 cm. In order to reduce the background from converting photons in the sample, the invariant mass of the pair calculated with the assumption that they are both electrons is required to be greater than 30 MeV/c<sup>2</sup> and the proper time of the  $K_S$  must be greater than 0.5 cm/c.

The efficiency is found from a sample of Monte Carlo events produced by the Ali Monte Carlo with initial state radiation. The distribution of produced K's is normalized to the measured distribution for  $p > 250$  MeV/c to find the number of K's produced below this cut.

Assuming standard branching ratios for  $K_S \rightarrow \pi^+\pi^-$  and an equal number of  $K_L$  and  $K_S$  mesons yields  $8332 \pm 663$  produced neutral K's for a total integrated luminosity of  $15.4 \text{ nb}^{-1}$ . The total cross section is therefore  $\sigma = 0.541 \pm 0.043 \pm 0.054 \text{ nb}$  and the average multiplicity of neutral K's is  $1.3 \pm 0.1$  per hadronic event. The systematic error of 10% comes from the luminosity normalization, the radiative corrections, and the Monte Carlo efficiency calculation.

The inclusive distribution in  $x$  for the neutral K's is compared to the same distribution for all charged particles in fig. 50. Although there is some increase in the K fraction as a function of  $x$ , the basic conclusion is that the slope of the two distributions are quite similar, and that therefore the production mechanisms for K's are similar to those of the pions which dominate the all charged distribution. K mesons which are decay products of heavy mesons ( $D \rightarrow K$  or  $B \rightarrow D \rightarrow K$ ) would tend to increase the K fraction at low  $x$  unless there were as many  $\pi$ 's produced as K's.

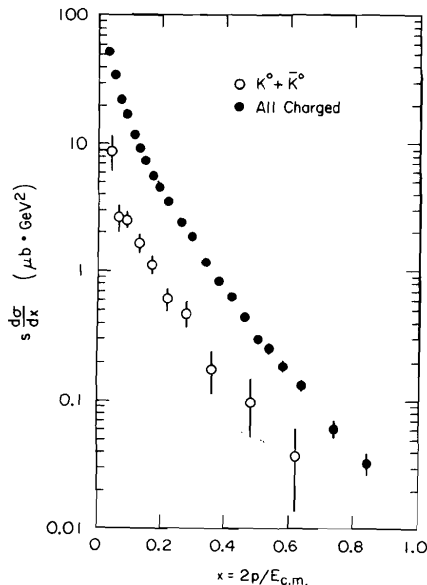


Fig. 50. Radiatively corrected inclusive  $x$  distribution for neutral K's and for all charged particles.

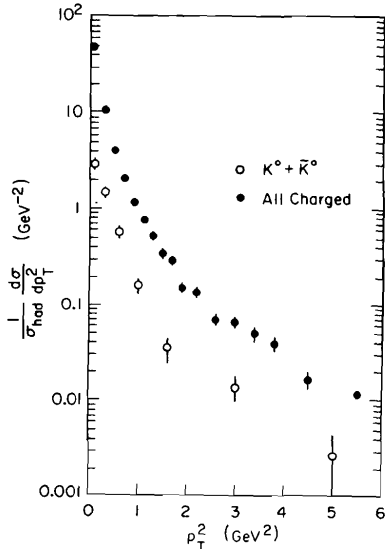


Fig. 51. Comparison of the  $p_T^2$  distribution for neutral K mesons and all charged showing jet broadening for K's.

By looking at the  $p_T^2$  behavior of the K mesons relative to the sphericity axis, we can find out whether gluons also produce K mesons. From the distribution shown in fig. 51 we learn that the same broadening in  $p_T^2$  which indicated the presence of gluon radiation in the charged particles is seen in the neutral K's. At high  $p_T^2$  the distributions are the same within statistics and hence the dynamics of gluon fragmentation into kaons must be very similar to that for pi mesons.

### Protons

Baryons are an interesting probe of the fragmentation process because it takes three quarks in a color singlet configuration to make a baryon. In an SU(3) symmetric fragmentation process, the multiplicity of quarks and gluons in a gluon jet is larger than that in a quark jet by the ratio of the color factors, namely  $9/4$ .<sup>29</sup> The increased number of quarks

might make it easier to obtain the three quarks required for a baryon in a gluon jet. Early measurements of the decays of the upsilon resonances, which are interpreted in QCD as three gluon decays, do in fact indicate an increase in baryons. The experiments, however, disagree on the magnitude of the effect.<sup>30,31,32</sup> At high energies, the increase in number and energy of the produced gluon jets should influence the baryon composition of annihilation events. The momentum spectrum of these baryons should give us further information about the dynamics of the fragmentation process.

Protons and antiprotons are identified in the MARK II detector by the time-of-flight scintillators.<sup>33</sup> The data are taken from a sample of 5500 hadronic events obtained at 29 GeV. Figure 52 shows a scatter plot of the invariant mass determined by the time-of-flight measurement for each particle versus the particle momentum  $p$ . Each scintillator used in these measurements is required to be hit by only one reconstructed track due to the difficulties of interpretation in the case of multiple hit counters. This results in a large loss (30%) of usable tracks compared to similar data taken by the same detector at SPEAR (5% loss) due to the increased multiplicity and decreased sphericity of events at 29 GeV. Protons and antiprotons are defined as tracks with a weight<sup>5</sup> greater than 0.5 for  $p \leq 1.4$  GeV/c and greater than 0.7 for  $1.4 < p \leq 2.0$  GeV/c. Figure 53 shows the difference between the expected and observed flight times of a well-separated sample of pions. The agreement of the shape of this distribution with the Monte Carlo curve indicates that

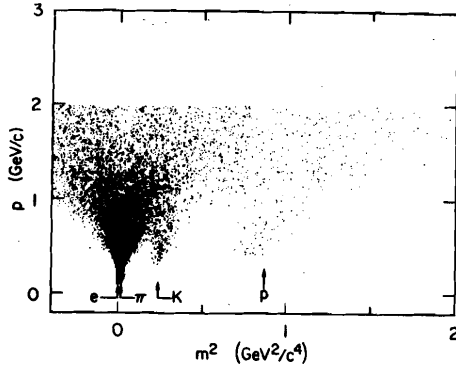


Fig. 52. Scatter plot of invariant mass determined by time-of-flight.

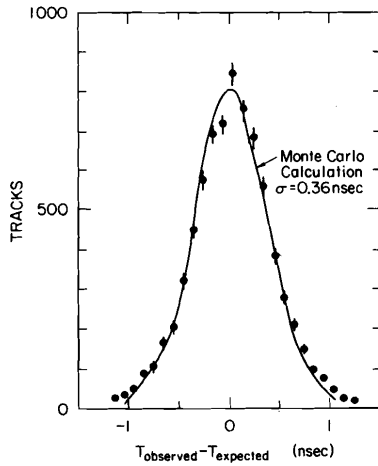


Fig. 53.  $T_{\text{observed}} - T_{\text{expected}}$  for pions compared to Monte Carlo simulation.

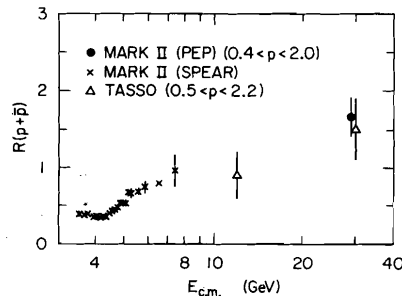


Fig. 54. Ratio of proton plus antiproton production to the  $\mu$  pair cross section for  $0.4 < p < 2$  GeV/c.

misidentification probabilities due to the cuts can be reliably calculated with the Monte Carlo.

The Ali Monte Carlo has been used to calculate the misidentification probabilities as a function of momentum, and a subtraction has been made from the observed spectra. Since this Monte Carlo does not include baryon production, it has been modified to include a probability  $P_B$  per jet of producing a diquark pair during the fragmentation process. The diquark fragmentation function is

$$a + (1 - a)(n + 1)(1 - x)^n$$

$$a = .3, \quad n = 2$$

The diquark transverse momentum is the same as that for the quarks (.3 GeV/c) and only octet baryons are generated and allowed to decay. To fit the observed number of produced baryons, this Monte Carlo model requires  $P_B = 0.115$ . The determination of the efficiency for finding protons and antiprotons within a jet is insensitive to the details of the Monte Carlo.

The ratio of the proton plus antiproton cross section within the momentum interval  $0.4 < p < 2.0$  GeV/c to the  $\mu$  pair cross section is shown in fig. 54. Under the assumption that the number of produced neutrons is equal to the number of produced protons, this ratio is also the ratio of nucleons plus antinucleons to  $\mu$  pairs. The value  $R(p + \bar{p})$  at 29 GeV is  $1.66 \pm 0.13$  indicating that baryon production is an important feature of these high energy events. Also shown in this figure are the results from the MARK II detector at SPEAR and the TASSO detector at 12 GeV<sup>34</sup> for the same momentum range.

Unfortunately the time of flight technique provides proton data over only a restricted momentum range. To correct for the part of the momentum range which is not observed, the invariant cross section  $E d^3\sigma/dp^3$  is usually fit to a function of the form  $e^{-bE}$ . It is then assumed that the cross section is independent of  $\cos\theta$  and the invariant cross section is found from

$$E \frac{d^3\sigma}{dp^3} = \frac{E}{4\pi p^2} \frac{d\sigma}{dp}$$

This of course assumes that the  $\langle p_{\perp} \rangle$  of the baryons is not limited relative to the jet axis. If the baryons were produced with  $\langle p_{\perp} \rangle \approx 0$ , they would have the  $1 + \cos^2\theta$  distribution of the primary quarks. This change in the  $\langle p_{\perp} \rangle$  dependence would result in a 14% change in the estimated cross section for all momenta. Since as we will see, the momentum distribution of the baryons is not well understood, it is more correct at this time to quote only the visible part of the cross section.

As discussed before, the momentum distribution of the baryons is sensitive to the details of the way in which they are produced in the fragmentation process. The cross-section for  $p + \bar{p}$  is shown in fig. 55 as a function of momentum together with earlier measurements by TASSO<sup>34</sup> and JADE<sup>35</sup> and the predictions of the LUND group.<sup>36</sup>

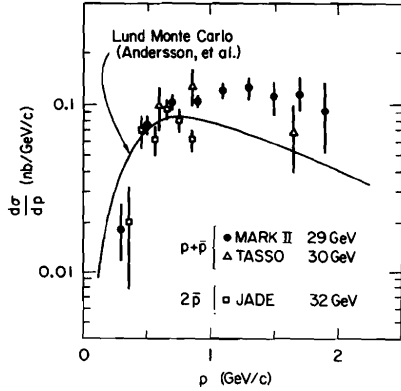


Fig. 55.  $\sigma(p+\bar{p})$  versus momentum from MARK II, TASSO and JADE with LUND prediction.

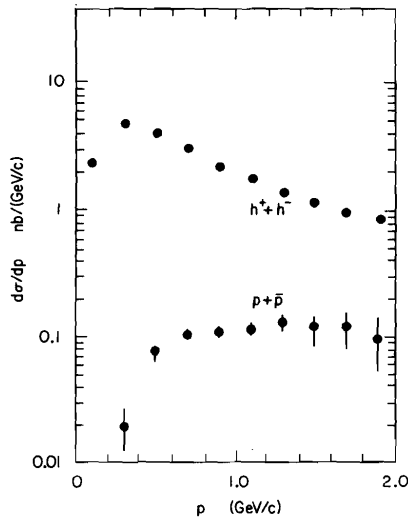


Fig. 56.  $d\sigma/dp$  for  $p+\bar{p}$  compared to all charged particles.

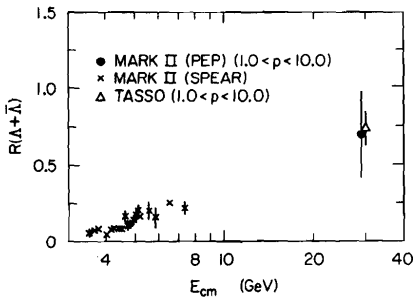


Fig. 57.  $R(\Lambda+\bar{\Lambda})$  for  $1.0 < p < 10.0$  GeV/c.

Although the LUND approach was consistent with the early results, it falls short of predicting the high momentum yield. The LUND approach is similar to the MARK II modifications of the Ali Monte Carlo and has a probability for diquark production  $P_B = 0.065$  which is determined by the behavior of  $R(p+\bar{p})$  at SPEAR energies. No adjustment of the parameters of this model has been tried yet. The MARK II--Ali Monte Carlo reproduces the correct total number of protons by using a higher value of  $P_B$ , but predicts a shape which is similar to that of the LUND model and is a poor fit to the data. The data show twice as many protons near 2 GeV/c compared to the model prediction. Therefore, the data are inconsistent with the naive assumptions which have so far been used in the baryon models and Monte Carols. With increased statistics, we will eventually be able to determine the extent to which the gluons in 3-jet events are contributing if at all to the baryon excess. Many other interesting tests such as the prediction of

$$\frac{q \rightarrow p}{q \rightarrow \pi^\pm} \sim (1-x)^2$$

$$\frac{q \rightarrow \bar{p}}{q \rightarrow \pi^\pm} \sim (1-x)^6$$

$$\frac{q \rightarrow p, \bar{p}}{q \rightarrow \pi} \sim (1-x)^2$$

derived from naive quark counting are difficult to test because of the restrictive momentum range of the time-of-flight technique. Figure 56 compares the behavior of  $d\sigma/dp$  for  $p+\bar{p}$  and all charged particles up to 2 GeV/c.

$\Lambda, \bar{\Lambda}$  results

The  $\Lambda, \bar{\Lambda}$  baryons can be detected by the MARK II detector using a technique which is similar to that used in finding the  $K_S^0$ . Pairs of particles are chosen which have a vertex at least 1.0 cm from the beam crossing point in three dimensions. The momentum of the candidate  $\Lambda$  must be at least 1 GeV/c and must be less than the beam energy. The angle between the momentum vector and the line joining the origin to the secondary vertex must satisfy  $\cos\theta < .98$ . Time-of-flight information is used to identify protons up to 1.6 GeV/c. For higher momenta, all tracks are tried as protons. Candidate  $\Lambda$ 's are selected from the mass range  $1.108 < m < 1.124$  GeV/c<sup>2</sup> and backgrounds are subtracted by looking at events on either side of the  $\Lambda$  peak. With these cuts, there are 172  $\Lambda+\bar{\Lambda}$  events over a background of 150 events.

The ratio of the total cross section observed in the momentum range  $1.0 < p < 10$  GeV/c to the  $\mu$  pair cross section is shown in fig. 57, together with lower energy measurements by the MARK II detector and the 30 GeV measurement of the TASSO collaboration. The value of  $R(\Lambda+\bar{\Lambda})$  at 29 GeV is  $0.73 \pm 0.11$ . To obtain the value of  $R(\Lambda+\bar{\Lambda})$  corrected for the full momentum range, the invariant cross section  $E d^3\sigma/dp^3$  is fit to the form  $e^{-bE}$ .

The value of the slope parameter is  $b = 0.82 \pm 0.09 \text{ GeV}^{-1}$ . As was discussed for the protons, there are uncertainties in this procedure, but since the  $\Lambda$ 's are measured over a larger momentum range than the protons, we have extrapolated the momentum spectrum and find  $R(\Lambda + \bar{\Lambda}) = 0.80 \pm 0.13$  for the full momentum range. The slope parameter measured in this momentum range disagrees with the value obtained for low momentum  $\Lambda$ 's ( $p < 1 \text{ GeV}$ ) by the JADE collaboration. They obtain a slope parameter which agrees within errors with the value  $b \approx 1.6 \text{ GeV}^{-1}$  obtained for low momentum protons (see fig. 58). If the invariant cross section actually had a change in slope from 1.6 below 2 GeV/c to 0.8 above, this would lead to a 40% increase in the extrapolated cross section.

The data obtained for neutral K's and for  $\Lambda$ 's allow us now to compare the momentum distributions of produced strange baryons and mesons. The momentum distribution  $d\sigma/dp$  is shown in fig. 59. There is a rapid rise in the strange baryon

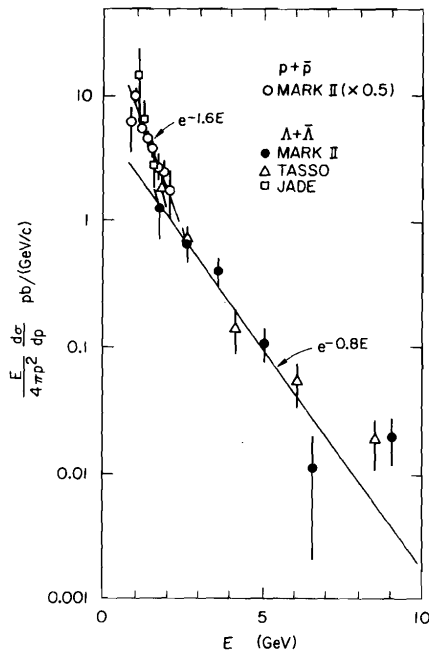


Fig. 58.  $E d^3\sigma/dp^3$  for  $\Lambda, \bar{\Lambda}$  and protons.

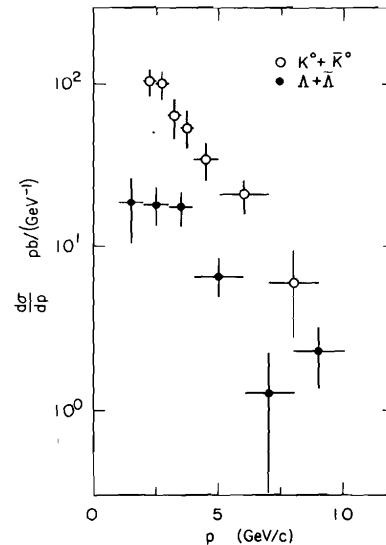


Fig. 59.  $d\sigma/dp$  for strange baryons and mesons.

to meson ratio at low momenta and then a slower rise for  $p > 3 \text{ GeV/c}$ . The slopes of high momentum parts of the distributions are within errors of being the same. With increased statistics, this comparison will become an interesting test of quark counting rules and quark fragmentation dynamics.

### Baryon pairs

Events in which a pair of baryons are detected provide a unique test of whether baryon number is conserved locally in the fragmentation process or globally. Models of the type which include diquark production in the fragmentation chain have local baryon number conservation and tend to produce baryon-antibaryon pairs which are in the same jet and have small rapidity gaps.

A preliminary analysis of the pair data for protons has led to two surprising observations. First, for baryon-antibaryon pairs there are approximately as many pairs observed in opposite jets and same side jets. The opposite jet component is not predicted by the LUND or MARK II type Monte Carlo. Second, there are a large number of same charge baryons again equally distributed between same side and opposite side jets. Baryon conservation requires that these events actually contain four baryons!

There are many problems in the analysis of this data and more definite answers will require additional systematic and background checks. One of the problems is of course that the time-of-flight technique for protons yields pairs only

in the soft region  $x < 0.14$ . To calculate the efficiency for finding pairs of protons, one must have a model which roughly reproduces the momentum correlations of the data. No model of baryon production yet describes the single proton momentum spectrum and the presence of opposite jet pairs indicates that the correlations are not well reproduced either. A further problem arises from the requirement in the proton analysis that the time-of-flight counters be hit only by a single track. At PEP energies this represents a 30% reduction in simple track efficiency and therefore a 50% reduction in the pair efficiency. For same jet pairs with small rapidity gaps such as would be produced by diquark models, the efficiency of this cut is sensitive to the rapidity gap distribution.

If one uses data which contain multihit counters, then one relies more heavily on the Monte Carlo simulation of the counter response, and as a result, the uncertainty in the feedthrough is increased. Tables 3 and 4 show the baryon pair samples obtained using these two techniques.

TABLE 3

Baryon Pairs using Multihit Counters;  
No Background Subtraction.

	Same Jet	Opposite Jet
$p\bar{p}$	40	29
$\bar{p}\bar{p} + pp$	19	22

TABLE 4

Baryon Pairs using Single Hit Counters,  
Background Subtracted.

	Same Jet	Opposite Jet
$p\bar{p}$	10	10
$\bar{p}\bar{p} + pp$	2	7

In summary, the particle separated cross sections provide interesting tests of the underlying dynamics of quark fragmentation. Comparisons of neutral K mesons with charged hadrons indicate very similar behavior for the K's including the observation of  $p_{\perp}$  broadening of the K's with respect to the sphericity axis. The proton data indicate several discrepancies between the naive expectations of diquark models. In particular, a mechanism will have to be found to stiffen the momentum distribution of the produced protons. Much work remains and the inclusion of charmed baryons and primary diquark production needs to be investigated. Interesting tests of gluon fragmentation will become available when there are sufficient statistics to see protons in the softest jet of three-jet events. Finally, the correlations of baryon pairs are an even more detailed test of the quark fragmentation and perhaps not surprisingly again disagree with models currently available.

#### OTHER HADRONIC PROPERTIES

There are several properties of hadron production at PEP which have been investigated where the analysis methods are well-known and where the results agree well with previous measurements by PETRA groups. The total hadronic cross section has been measured by both the MAC and MARK II groups. For the ratio R of this cross section to the  $\mu$  pair cross section at 29 GeV, the MAC group obtains

$R = 3.5 \pm 0.4$  and the MARK II group obtains  $R = 4.02 \pm 0.10 \pm 0.35$ . In the latter case the systematic error is dominated by an estimated 5% uncertainty from the luminosity and 7% from the efficiency corrections. Both groups are investigating the possibilities of reducing these systematic errors.

The MARK II group has also measured the mean charged multiplicity and finds  $\langle n_{CH} \rangle = 12.0 \pm 0.6 \pm 1.2$ . Figure 60 shows the sphericity distribution from the MARK II data. The mean value of sphericity is a test for the presence of a top quark. The mean value for the data is  $\langle S \rangle = 0.130 \pm 0.003$  to be compared with an expected value  $\langle S \rangle = 0.24$  if the top quark were present. The shape of the sphericity distribution agrees with that measured by the TASSO group at 30 GeV.

The behavior of the cross section  $d\sigma/dp_{\perp}^2$  where  $p_{\perp}$  is measured relative to the

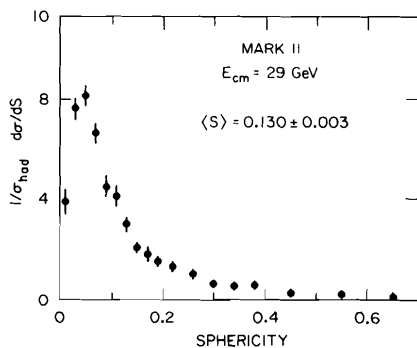


Fig. 60. Sphericity distribution at 29 GeV.

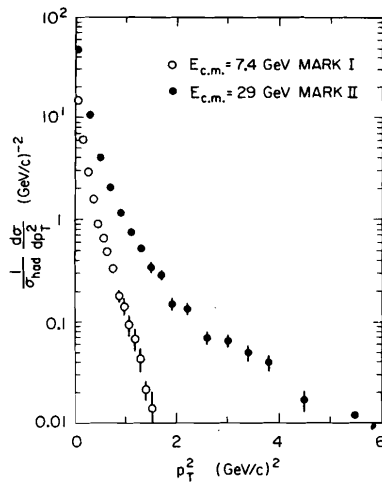


Fig. 61. Comparison of  $d\sigma/dp_T^2$  at low and high energies showing jet broadening.

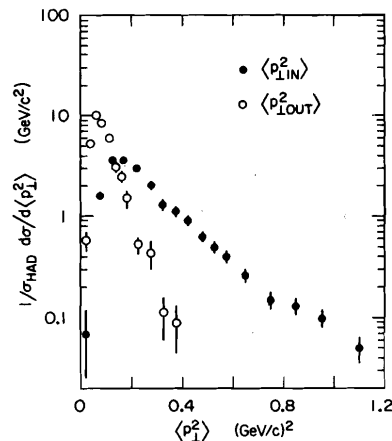


Fig. 62.  $d\sigma/d\langle p_1^2 \rangle$  in and out of the event plane. Broadening is observed in the event plane.

$2\pi^+2\pi^-$  was large even below the  $\rho\rho$  threshold. The MARK II measurements at PEP confirm this behavior. Theoretical calculations have so far failed to explain this behavior. A perturbative QCD calculation<sup>40</sup> for  $\gamma\gamma + \rho\rho$  gives a cross section of 20 nb at 1.5 GeV. Vector meson dominance predicts a value of approximately 30 nb in this region. It has also been suggested<sup>41</sup> that there may be a new resonance at 1.6 GeV/c<sup>2</sup> but the detailed explanation of the cross section requires the inclusion of a large final state interaction between the  $f(1270)$

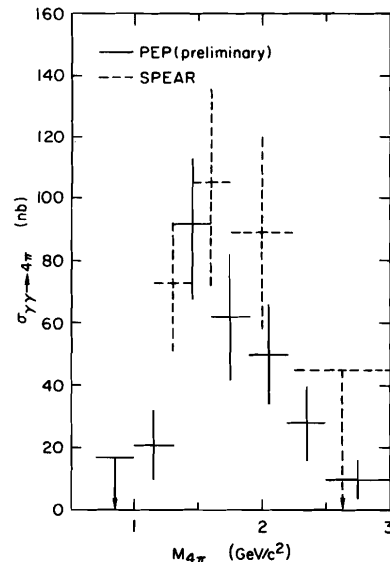
Fig. 63. Two photon production of  $2\pi^+2\pi^-$  as measured at SPEAR and PEP.

sphericity axis is sensitive to the jet behavior of hadron production and was one of the first indications that  $\langle p_1^2 \rangle$  was increasing with energy due to gluon emission. Figure 61 compares the cross section obtained at high energies by the MARK II detector with that obtained at low energies by the MARK I detector. It is clear that there has been a substantial change in this cross section.

Further evidence for the gluon emission model comes from the observation of the planarity of the hadronic events. Two jet events from  $q\bar{q}$  initial states would not be expected to exhibit any planar behavior, but three body states such as  $q\bar{q}g$  should have a planar structure with larger  $\langle p_1^2 \rangle$  in the event plane than out of the event plane. The distribution in  $\langle p_1^2 \rangle$  in the event plane and out of the event plane are compared in fig. 62. The behavior of  $\langle p_1^2 \rangle$  in the event plane is the same as that observed at low energies which indicates that the growth in  $p_1$  observed in fig. 61 is due mainly to planar events. Again these distributions are in good agreement with previous results.<sup>37</sup>

Finally, in the coming months further information will become available on the production of hadrons via the interaction of two virtual photons. Often considered a background by those interested in hadronic final states, this process will allow a systematic investigation of low energy  $C = +1$  resonance states. Difficulties in the interpretation of this data arise primarily from the uncertain energy and momentum of the initial state when the two scattered electrons are undetected. Detection of these electrons is difficult and greatly reduces the detection efficiency for these final states. Recent emphasis has therefore been placed on the exclusive production of resonance states. As an example of this technique, the MARK II collaboration has made a preliminary measurement of the four-charged-pion final state. Figure 63 shows the comparison of the two photon production of  $2\pi^+2\pi^-$  with earlier data obtained at SPEAR by the same detector.

The TASSO collaboration<sup>38</sup> was the first to observe that there was a large two photon cross section near the  $\rho\rho$  threshold. Measurements at SPEAR by the MARK II<sup>39</sup> group indicated that the cross section for



and  $\epsilon(1300)$  mesons. These authors point out that the investigation of the behavior of  $\omega\omega$ ,  $K^*K^*$ ,  $\rho\gamma$  and other two-body final states can be used to clarify the situation. Clearly there is much work to be done and much to learn in this field.

#### SUMMARY

QED reactions at high energies continue to provide tests of this remarkably successful theory. New limits have been obtained for possible breakdown effects in the reaction  $e^+e^- \rightarrow \gamma\gamma$  by the MAC and MARK II groups. No deviations from the expected behavior have been seen. Investigations of possible weak interference effects in  $e^+e^- \rightarrow \mu^+\mu^-$  and changes in the shape and normalization of  $e^+e^- \rightarrow e^+e^-$  have been performed and have reached the point where gauge theories of the Weinberg-Salam type are preferred at about the one sigma level. The  $\tau$  pair cross section has been measured to large values of  $|\cos\theta|$  by the MAC collaboration and agrees well with the expected  $1+\cos^2\theta$  behavior of QED.

Searches for additional sources of lepton production either from heavy leptons or excited states of the muon decaying via  $\mu^* \rightarrow \mu\gamma$  show no evidence for any anomalies and limits have been placed on the mass of a heavy lepton at  $14 \text{ GeV}/c^2$  and on the cross section and branching ratios for  $\mu^*$ 's. Again, conventional sources from QED explain all of the data.

The  $\tau$  lifetime has been measured for the first time by the MARK II group and the value obtained agrees well with that calculated from  $\tau$ - $\mu$  universality. Further improvements to the MARK II detector in the summer of 1981 will continue to improve this test of the coupling of the  $\tau$  to the weak charged current.

Scaling violations in the inclusive production of hadrons have been seen by comparing the data taken by the MARK II detector at SPEAR and at PEP. The qualitative features of the scale violation agree with the expected depletion at high  $x$  and  $s$  in QCD but a detailed test of QCD will require further understanding of the charm quark fragmentation function.

Tests of QCD have been made using distributions which are as much as possible independent of Monte Carlo calculations. The energy-energy correlations have been measured using both charged and neutral particles and the results agree in shape with perturbative QCD calculations. The normalization of the energy-energy correlations has been used to determine the value of the QCD coupling constant  $\alpha_s = 0.18 \pm 0.015 \pm 0.03$ . Further tests of QCD have been investigated using energy weighted cross sections in a single jet. The jet calculus approach using leading log QCD has been compared to the data and the agreement with the measured cross sections is good. Using the formalism of the jet calculus, the  $Q^2$  behavior of  $\alpha_s$  can be determined and the data indicates a growth of  $\alpha_s$  at low  $Q^2$  which is in good agreement with the theory.

Three-jet events in the MARK II detector have been used to test for sensitivity to the gluon spin using the method of Ellis and Karliner. A gluon spin of one is preferred by the data. Difficulties with measuring the detailed properties of the lowest energy jet to separate the behavior of gluon and quark fragmentation properties have been pointed out. The behavior of the lowest energy jet in  $p_1$  is found to be the same as that for quark jets at the same average energy.

The spectrum of produced  $K^0$  mesons has been measured and the  $s d\sigma/dx$  and  $d\sigma/dp_1^2$  behavior are found to be similar to that of all charged particles. The  $p_1$  broadening observed for all charged particles is also seen for the  $K^0$ 's indicating that gluons are also responsible for K meson production.

Proton and  $\Lambda$  production have also been investigated. Here the agreement between known models of baryon production and the data is less satisfactory. The measured cross sections for baryon production are higher than predicted by the models especially for protons with momenta between 0.9 and 2.0  $\text{GeV}/c$ . The correlations observed in proton pair production show large numbers of same sign and opposite jet pairs despite the tendency of diquark models to produce same jet opposite charge pairs.

Many other features of hadronic production have been investigated and excellent agreement is found with previous results of PETRA experiments. It is clear that high energy  $e^+e^-$  annihilation remains a fruitful testing ground for theories of the weak, electromagnetic and strong interactions. Much remains to be learned, and we can look forward to many further interesting results in the coming year.

## REFERENCES

- (1) M. Capdequi-Peyraneyre et al., Montpellier PM/80/9 (1980).
- (2) F. A. Berends, R. Kleiss, DESY Report 80-66 (1980), and Nucl. Phys. B 186 (1981) 22.
- (3) P. Dittman, V. Hepp, DESY 81/030 (June 1981).
- (4) R. Budny, Phys. Lett. 55B (1975) 227.
- (5) J. Kim, P. Langacker, M. Levine, H. Williams, Rev. Mod. Phys. 53 (April 1981) 211.
- (6) J. Ellis et al., Nucl. Phys. B 182 (1981) 529; A. Ali, DESY 81/032 (June 1981).
- (7) Previous experiments have reported upper limits for the  $\tau$  lifetime. See R. Brandelik et al., Phys. Lett. 92B (1980) 199.
- (8) A. Ali et al., Phys. Lett. 93B (1980) 155.
- (9) G. Hanson, 13th Rencontre de Moriond (1978); ed. J. Tran Thanh Van, Vol. III.
- (10) R. Brandelik et al., Phys. Lett. 89B (1980) 418.
- (11) G. Altarelli, O. Parisi, Nucl. Phys. B 126 (1977) 298.
- (12) P. Soeding, G. Wolf, DESY 81-013 (1981).
- (13) G. Sterman, S. Weinberg, Phys. Rev. Lett. 39 (1977) 1436; G. Fox, S. Wolfram, Nucl. Phys. B 149 (1979) 413.
- (14) C. Basham, L. Brown, S. Ellis, S. Love, Phys. Rev. D 17 (1978) 2298.
- (15) C. Basham, L. Brown, S. Ellis, S. Love, Phys. Rev. D 19 (1979) 2018.
- (16) C. Basham, L. Brown, S. Ellis, S. Love, Phys. Rev. Lett. 41 (1978) 1585.
- (17) PLUTO collaboration (Ch. Berger et al.), Phys. Lett. 99B (1981) 292.
- (18) G. Sterman, S. Weinberg, Phys. Rev. Lett. 39 (1977) 1436.
- (19) K. Konishi, A. Ukawa, G. Veneziano, Nucl. Phys. B 157 (1979) 45; K. Konishi, CERN TH 2853 (1980) and CERN TH 2892 (1980).
- (20) R. K. Ellis, R. Petronzio, Phys. Lett. 80B (1979) 249; G. Curci, M. Greco, Phys. Lett. 79B (1979) 406.
- (21) J. Dorfan, Z. Phys. C 7 (1981) 349.
- (22) H. Daum, H. Meyer, J. Burger, DESY 80/101.
- (23) S. Brandt, H. Dahmen, Z. Phys. C 1 (1979) 61.
- (24) S. Wu, G. Zoernig, Z. Phys. C 2 (1979) 207.
- (25) J. Ellis, M. Gaillard, G. Ross, Nucl. Phys. B 111 (1976) 253.
- (26) J. Ellis, I. Karliner, Nucl. Phys. B 148 (1979) 141.
- (27) R. Brandelik et al., Phys. Lett. 97B (1980) 453.
- (28) Ch. Berger et al., DESY 80/93 (1980).
- (29) S. Brodsky, J. Gunion, Phys. Rev. Lett. 37 (1976) 402; See also B. Anderson et al., LUND LU TP 81-3 (April 1981).
- (30) H. Albrecht et al., Phys. Lett. 102B (1981) 291.
- (31) M. Gilchriese, SLAC Summer Institute (August 1981).
- (32) J. Bienlein, this conference.
- (33) G. Abrams et al., Phys. Rev. Lett. 44 (1980) 10. J. Weiss et al., Phys. Lett. 101B (1981) 439.
- (34) R. Brandelik et al., Phys. Lett. 94B (1980) 444.
- (35) W. Bartel et al., DESY 81-028 (June 1981).
- (36) B. Anderson et al., LUND LU TP 81-3, April (1981).
- (37) For reviews of PETRA data see:  
G. Wolf, DESY 80/13 (February 1980).  
B. Wiik, DESY 80/129 (December 1980).  
S. Wu, DESY 81-003 (January 1981).  
P. Söding, G. Wolf, DESY 81-013 (March 1981).  
H. Meyer, Wuppertal Print 81-0574 (August 1981).
- (38) R. Brandelik et al., Phys. Lett. 97B (1980) 448.
- (39) D. L. Burke et al., SLAC-PUB-2693 (1981).
- (40) S. Brodsky, P. Lepage, SLAC-PUB-2587 (1981).
- (41) J. Layssac, F. M. Renard, MONTPELLIER Preprint PM/80/11 and PM/81/5.

## FOOTNOTE

\* Work supported by the Department of Energy, contract DE-ACO3-76SFO0515.

## DISCUSSION

- Q. J. Kirkby :  
(Stanford) Regarding  $\tau$  lifetime, in the plot you show of about 100 events there are three events at 20 mm. If I give these the benefit of a positive measurement of  $2\sigma$ , then I would place them at 12 mm. Its still about 15  $\tau$  lifetimes and it must have a big effect on the likelihood function weighting. Now if those events were to be dropped, what would the answer be? Would it make your  $2\sigma$  measurement a  $1\sigma$  measurement?
- R. Hollebeek : The answer is NO. Note that only one of the three events remains in the high resolution sample. When one does the maximum-likelihood fit, each event has a weight which goes into the determination of the  $\tau$  lifetime. This weight is determined by the full error matrix from the vertex fit. In addition, the likelihood function contains a flat contribution from background events and the measurement is not pulled by the events in the tail of the distribution.
- Q. B. Esposito :  
(CERN) What is the average  $p_{\perp}^2$  in the hadronic events?
- R. Hollebeek : It agrees very well with the PETRA result. The distributions agree almost exactly. There is good agreement between MARK I and MARK II at low energies and in the MARK II data at low and high energies we see the same  $p_{\perp}$  broadening observed at PETRA.
- P. Söding :  
(DESY) The average value of  $p_{\perp}^2$  found by TASSO is  $0.31 \text{ GeV}^2$  at  $W \sim 30\text{-}35 \text{ GeV}$ . This is an average over final hadrons and therefore is dominated by low momentum fragments. Thus, this number by itself is not very significant for QCD effects; to see these, one has to look into the tail of the  $p_{\perp}^2$  distribution.
- Q. G. Knies :  
(DESY) What is the average rapidity gap of the same side and opposite side pp pairs?
- R. Hollebeek : As I said, we see a lot of protons at high momentum and we see them in both the same and opposite jets. What happens when one goes ahead and makes a rapidity distribution is that one sees a set of events which cluster at low rapidity gaps and a set of events which come from the high momentum p's in opposite jets which cluster at high rapidity gaps. The problem is that it is difficult to correct that distribution and come out with a rapidity gap distribution because one doesn't know anything about the  $p_{\perp}^2$  behavior for fixed rapidities. Until we have a large enough sample to actually see the cross section in  $d\sigma/dp_{\perp}^2$  for the baryons, or until we have some model that models the momentum behavior better than we have, we can't make those corrections.
- Q. G. Barbiellini :  
(CERN) The TASSO momentum distribution for  $\Lambda$ 's gives  $b = 2.5 \text{ GeV}$ . Is this in disagreement with your proton distribution?
- R. Hollebeek : With the proton distribution, yes.
- Q. J. Rohlf :  
(Harvard) On the  $\tau$  lifetime, do you use 6 prongs and how do you separate those from hadronic events?
- R. Hollebeek : This is not a problem because you require the invariant mass to be very low and the separation is quite good. In the total sample about 10% are 6-prong events.

Q. M. Gilchriese : Can you compare  $\langle p_1 \rangle$  or  $\langle p_1^2 \rangle$  in the third jet with PETRA data?  
(Cornell)

R. Hollebeek : If you do it as a function of energy of the jet calculated from the jet angles, you will find that as with  $\langle n_{CH} \rangle$  there is no overlap so you can't draw any conclusions. When we made the same distribution using energy calculated from the visible energy, we found results that are qualitatively similar to what our PETRA colleagues find. However, it is well known that  $\langle p_t \rangle$  and  $\langle p_t^2 \rangle$  are functions of energy and so one has to compare two jets at the same energy. Using visible energy tends to bias the energy measurement.

Q. H. Newman : In the determination of  $\alpha_s$  from the energy correlations, you looked at the  $\cos\theta$  moments and compared it to jet calculations. How would these effects be modified by things which are outside the theory such as heavy quark masses and weak decays?  
(DESY)

R. Hollebeek : The measurement itself is not affected whatsoever and its up to the theorist to answer the question why the model, which doesn't include any of these effects, explains the data reasonably well. That's one of the advantages of this type of measurement--the data stands on its own and we hope there will be some progress in the calculations.

Q. H. Newman : That's true as long as one doesn't quote a value of  $\alpha_s$  from this analysis.

Q. H. Meyer : You determine that  $Q^2$  dependence of  $\alpha_s$  from this energy distribution in a single jet. Have you tried to compare this result to a calculation ala Field-Feynman, for example?  
(Wuppertal)

R. Hollebeek : We have looked at the behavior of the lowest moment,  $C_2$  in data generated by the Ali Monte Carlo which is basically the Feynman-Field Monte Carlo for the 2-jet sample. In that case, one finds that the behavior is qualitatively similar and that if one turns the crank and deduces  $\alpha_s$ , one finds that it runs. I think that's not terribly surprising. After all, Feynman-Field is supposed to describe the behavior of QCD at low  $p_t$ , so the fact that one has limited  $p_t$  behavior at low  $Q^2$  indicates that there is, in fact, a  $p_t$  scale which is important and one will see the sort of effects that correspond to having some sort of fixed scale or  $\Lambda$  value.